Kaposi's sarcoma-associated herpesvirus (KSHV) utilizes the NDP52/CALCOCO2 selective autophagy receptor to disassemble processing bodies

Short title: Selective targeting of processing bodies for autophagy by KSHV

inflammatory cytokine transcripts / Kaposi's sarcoma-associated herpesvirus / NDP52 / processing bodies / selective autophagy

Carolyn-Ann Robinson[1,2,3,4,5], Gillian K. Singh[1,5], Mariel Kleer[2,3,4], Elizabeth L. Castle[1,3], Bre Q. Boudreau[1], Jennifer A. Corcoran[1,2,3,4*]

[1]Department of Microbiology & Immunology, Dalhousie University, Halifax, NS, Canada
[2]Microbiology, Immunology & Infectious Diseases Department, University of Calgary, Calgary, AB, Canada.
[3]Charbonneau Cancer Research Institute, University of Calgary, Calgary, AB, Canada.
[4]Snyder Institute for Chronic Diseases, University of Calgary, AB, Canada.
[5]Equal Contribution
[*]Corresponding Author

Abstract

Kaposi's sarcoma-associated herpesvirus (KSHV) causes the inflammatory and angiogenic endothelial cell neoplasm, Kaposi's sarcoma (KS). We previously demonstrated that expression of the KSHV protein, Kaposin B (KapB), promoted inflammation via the disassembly of cytoplasmic ribonucleoprotein granules called processing bodies (PBs). Processing bodies (PBs) modify gene expression by silencing or degrading labile messenger RNAs (mRNAs) including many transcripts that encode inflammatory or angiogenic proteins that are associated with KS disease. Although our work implicated PB disassembly as one of the causes of inflammation during KSHV infection, the precise mechanism used by KapB to elicit PB disassembly was unclear. Here we reveal a new connection between the degradative process of autophagy and PB disassembly. We show that both latent KSHV infection and KapB expression enhanced autophagic flux via the phosphorylation of the autophagy regulatory protein, Beclin 1. KapB was necessary for this effect, as infection with a recombinant virus that does not express the KapB protein did not induce Beclin 1 phosphorylation or autophagic flux. Moreover, we reveal that PB disassembly mediated by KSHV or KapB depended on canonical autophagy genes and the selective autophagy receptor *NDP52/CALCOCO2* and that the PB scaffolding protein, Pat1b, co-immunoprecipitated with NDP52. These studies reveal a new role for autophagy and the selective autophagy receptor NDP52 in promoting PB turnover and the concomitant synthesis of inflammatory molecules during KSHV infection.

Author Summary

Kaposi's sarcoma-associated herpesvirus (KSHV) is the causative agent of the inflammatory, endothelial cell cancer, Kaposi's Sarcoma (KS). KSHV induces a pro-tumourigenic inflammatory environment which aids in the establishment and maintenance of the KS lesion. Processing bodies (PBs) are cellular structures that dampen inflammatory gene expression by suppression or decay of their cognate RNA molecules. We previously showed that the viral protein KapB caused PB disappearance during KSHV infection, identifying a new pathway used by KSHV to elicit inflammation. Now, we show that KSHV and KapB hijack the cellular degradative process of autophagy to promote PB disassembly and increase inflammatory gene expression. This places autophagy as central to the regulation of inflammation by KSHV and illustrates another remarkable strategy used by these viruses to create a tumourigenic microenvironment.

34 **Introduction**

35 Macroautophagy, hereafter referred to as autophagy, is an evolutionarily conserved degradative
36 process that ensures the continuous recycling of material to maintain cellular homeostasis (1–3).
37 Autophagy begins with the formation of a phagophore that elongates and encloses a portion of
38 the cytoplasm to form a double-membrane organelle, the autophagosome, which fuses with
39 lysosomes to form autolysosomes, where contents are degraded (4). Under basal conditions,
40 autophagic activity ensures the clearance of damaged macromolecular complexes and organelles,
41 acting as an intracellular quality control system to maintain homeostasis (2). Various changes to
42 the cellular microenvironment, including nutrient scarcity, hypoxia, and endoplasmic reticulum
43 (ER) stress can upregulate autophagy, reprioritizing resources and promoting cell survival during
44 adverse and stressful conditions (2).

45

46 Although previously considered a non-selective bulk degradative pathway of cytoplasmic
47 recycling, recent work shows differential cargo targeting by autophagy through a process known
48 as selective autophagy (5,6). Autophagy can selectively target specific cellular components,
49 including organelles (e.g mitochondria, peroxisomes, ER) and protein complexes (e.g.
50 ribosomes, focal adhesion complexes, protein aggregates) for degradation (5,7). In selective
51 autophagy, target cargo is either selected directly, by binding to lipidated microtubule associated
52 protein 1 light chain 3 (LC3) protein (LC3-II)/Atg8, or via a receptor that mediates cargo
53 recognition. These molecular bridges are termed selective autophagy receptors (SARs), and their
54 role is to link the selected cargo to lipidated LC3-II molecules which are anchored to the
55 expanding phagophore (8). Some of the best characterized SARs include p62/SQSTM1, valosin
56 containing protein (VCP), optineurin (OPTN), neighbor of BRCA1 gene 1 (NBR1), nuclear dot

57 protein 52 (NDP52/calcium binding and coiled-coil domain protein, CALCOCO2) and its
58 paralogue TAX1BP1/CALCOCO3 (5,9,10). Of these, OPTN, p62, NDP52, and NBR1 are
59 members of the sequestosome-like family and contain several conserved motifs including a LC3-
60 interacting region (LIR) and a ubiquitin-binding domain (UBD) to mediate cargo selection via
61 binding ubiquitin chains present on the cargo surface (6,11–13).
62
63 While SARs play important homeostatic roles maintaining, and at times magnifying, the turnover
64 of organelles and aggregates via cargo selection, emerging functions of these receptors is to
65 localize the initiation of autophagy and modulate cellular signalling. SARs p62 and NDP52 both
66 promote autophagosome formation at the cargo site through direct interactions with autophagic
67 initiating complexes (14–16). SARs also play important roles in fine-tuning innate immune
68 responses by targeting key signaling platforms for degradation (17–22). For example, NDP52 is
69 required for the autophagic degradation of interferon regulatory factor 3 (IRF3) and
70 mitochondrial antiviral signaling protein (MAVS), which supports the resolution phase of type I
71 interferon signaling (19,23,24). Selective autophagy can also degrade invading pathogens such
72 as viruses in a process called xenophagy (25). Both proviral and antiviral roles have been
73 attributed to SARs (26,27) and viruses can both enhance or limit SAR function accordingly,
74 promoting their replication (28).
75
76 Kaposi's sarcoma-associated herpesvirus (KSHV) is the infectious cause of two B-cell
77 malignancies and the endothelial cell cancer, Kaposi's sarcoma (KS), which features aberrant
78 angiogenesis, tortuous leaky blood vessels, and inflammation (29–31). Infection with KSHV has
79 two forms, a latent phase and a lytic phase and it is the latent phase that predominates in KS

80 tumours (32–34). Like many viruses, KSHV manipulates the autophagic machinery. During
81 latency, the viral FLICE inhibitory protein (v-FLIP) binds Atg3 to suppress the LC3 lipidation
82 process during autophagosome biogenesis (35). KSHV also expresses a viral cyclin D homolog
83 (v-cyclin), that triggers DNA damage leading to autophagy and cellular senescence (36),
84 facilitating the production and non-conventional secretion of pro-inflammatory cytokines/
85 chemokines such as IL-1β, IL-6 and CXCL8 (37). KSHV manipulation of autophagic flux
86 prevents xenophagy, limits interferon responses, and enhances inflammatory cytokine
87 production. Precisely how KSHV fine-tunes autophagy during latency to balance proviral and
88 antiviral activities and promote inflammation and chronic viral infection is not clear.
89
90 Processing bodies (PBs) are ubiquitous, cytoplasmic, ribonucleoprotein (RNP) granules that
91 regulate expression of many cytokine RNA transcripts, making them important sites of
92 inflammatory control. PBs contain enzymes involved in mRNA turnover, including those that
93 mediate mRNA decapping (Dcp2; co-factors Dcp1a, Pat1b and Edc4/Hedls), 5'-3'
94 exonucleolytic degradation (5'-3' exonuclease Xrn1 and RNA helicase Rck/DDX6) and some
95 components of the RNA-induced silencing complex (28,38–44). mRNAs are routed to PBs for
96 decay and/or repression by RNA-binding proteins (RBPs) through recognition of common
97 sequence elements (39). AU-rich elements (AREs) are destabilizing RNA regulatory elements
98 found in the 3' untranslated regions (UTRs) of ~8% of cellular transcripts that are responsible for
99 targeting RNAs to PBs (45–47). When bound by destabilizing RBPs, ARE-containing RNAs are
100 directed to PBs and suppressed (48–50). Our group and others showed that PB size and numbers
101 correlate with the constitutive turnover or translational suppression of ARE-mRNAs; when PBs
102 are dispersed, this suppression is reversed (51–55). Because ARE-mRNAs encode potent

103 regulatory molecules such as inflammatory cytokines, PBs are important post-transcriptional
104 sites of regulation that fine-tune the production of inflammatory cytokines whose transcripts
105 contain AREs, including IL-6, CXCL8, IL-1β, and TNF (46,56–62).
106
107 PBs are dynamic structures that are continuously assembled and disassembled, yet relatively
108 little is known about how their activity is regulated. Stimuli that activate the p38/MK2 MAP
109 kinase pathway as well as many virus infections elicit PB disassembly and a concomitant
110 reduction in ARE-mRNA suppression to promote inflammatory molecule production
111 (51,52,55,63–65). We have previously shown that KSHV causes PB disassembly during latent
112 infection, and that the viral protein Kaposin B (KapB) induces PB disassembly while enhancing
113 the production of an ARE-containing reporter (52,63,66). These data support the notion that PB
114 disassembly is likely an important contributor to inflammation associated with KS (52,67).
115 Although we know that KapB binds and activates the kinase MK2, and that MK2 is an important
116 component of the mechanism of KapB-mediated PB disassembly and ARE-mRNA stabilization,
117 we do not precisely understand how PB loss is elicited by KapB (52,68). The observation that
118 MK2 can phosphorylate the autophagy regulatory protein Beclin 1 to increase autophagic flux in
119 response to nutrient scarcity (69) suggested to us that KapB may drive autophagic flux through
120 MK2. We now show that the KSHV KapB protein enhances autophagic flux via the
121 phosphorylation of Beclin 1, and that KSHV infection also enhances autophagic flux and Beclin
122 1 phosphorylation in a KapB-dependent manner, revealing an additional layer of complexity in
123 viral regulation of autophagy during KSHV latency. We show that both KSHV infection and
124 KapB alone require autophagy proteins including the selective autophagy receptor, NDP52, to
125 induce PB disassembly and that KapB requires NDP52 to elevate selected ARE-containing

126 mRNA transcripts. PB turnover is likewise elicited by the mTOR inhibitor and potent autophagy
127 inducer, Torin-1, and this process is also dependent on Atg5 and NDP52. Finally, we show that
128 NDP52 co-immunoprecipitates with the PB scaffolding protein, Pat1b, providing a molecular
129 basis for the recognition of a PB component by NDP52. These data forge a new connection
130 between the selective autophagy receptor NDP52 and cytoplasmic PBs and show that selective
131 autophagy of PBs is promoted by the viral protein KapB during KSHV infection.
132

133 **Results**

134 **KapB induces autophagic flux**

135 KapB expression activates the stress-responsive kinase MAPKAPK2 (MK2) (52,68). Since MK2
136 phosphorylates the essential autophagy inducer Beclin 1 in response to amino acid starvation
137 (69–71), we questioned whether KapB expression could promote autophagic flux. Essential for
138 autophagosome expansion is the lipidation of LC3 to form LC3-II, permitting its incorporation
139 into autophagosome membranes where it is degraded along with autophagosomal contents in the
140 final step of autophagy (72). Since p62 is a selective autophagy receptor (SAR) that delivers
141 target cargo to the autophagosome, p62 is also degraded during the final step of autophagy. If
142 autophagic flux is elevated, blocking autophagic flux with a lysosomal inhibitor should result in
143 an accumulation of both p62 and LC3-II (73). To measure autophagic flux, we examined levels
144 of LC3-II and p62 with and without treatment with the lysosomal inhibitor, Bafilomycin A1
145 (BafA1). Human umbilical vein endothelial cells (HUVECs) were transduced with lentiviral
146 vectors that express KapB or an empty vector control and treated for increasing times with
147 BafA1. As expected, LC3-II and p62 accumulated in the presence of BafA1 treatment, and both
148 proteins showed higher accumulation after BafA1 treatment in KapB-expressing cells than
149 equivalently treated vector controls (Fig 1A), indicating that autophagic flux was enhanced in
150 KapB-expressing cells compared to vector controls. When KapB-expressing cells were treated
151 for 4 h with BafA1, the amount of LC3-II and p62 increased two- and four-fold, respectively
152 (Fig 1A). We also measured the formation of LC3 puncta as an indicator of autophagic flux by
153 staining KapB-expressing cells treated with BafA1 for endogenous LC3 (74,75). Untreated
154 KapB-expressing HUVECs displayed LC3 puncta area that was similar to that of control cells;
155 however, LC3 puncta area significantly increased after BafA1 treatment in KapB-expressing

156 cells and not in control cells, further suggesting that KapB expression enhanced autophagic flux
157 (Fig 1B).
158
159 **KapB-mediated PB disassembly requires Atg5 and Atg14**
160 Our group previously described that MK2 activation was an important component of KapB-
161 mediated PB loss (52); however, these experiments did not reveal the precise mechanism of PB
162 loss. Since PBs are dynamic RNP granules, we wanted to determine whether KapB-mediated PB
163 loss was a result of enhanced disassembly of PBs or prevention of their *de novo* assembly. To do
164 so, we utilized HeLa cells that express a Dox-inducible GFP-tagged version of the PB-resident
165 protein, Dcp1a (41). When fixed, GFP-positive puncta co-stain with endogenous PB proteins
166 such as the RNA helicase DDX6/Rck and the decapping co-factor Hedls/Edc4, indicating that
167 they represent PBs (Fig S1). KapB was transfected into these cells either before or after inducing
168 GFP-Dcp1a granule formation. When KapB was expressed prior to granule induction, Dcp1a
169 puncta formed, although appearance of GFP-positive puncta was delayed compared to vector
170 control cells (Fig S1A). In the presence of KapB, *de novo* PB assembly was not blocked;
171 however, when KapB was expressed after PB induction, GFP-positive puncta were lost (Fig
172 S1B), indicating that KapB expression induced PB disassembly. As further evidence that KapB
173 does not prevent PB formation, we treated KapB-expressing HUVECs with sodium arsenite, a
174 known inducer of PB assembly (76). Sodium arsenite induced endogenous PB formation in
175 KapB-expressing HUVECs was not significantly different from equivalently treated control cells
176 (Fig 1C). Taken together, these results show that KapB expression caused PB disappearance by
177 inducing PB disassembly but did not block PB assembly. We speculated that KapB may be

178 utilizing a normal cellular pathway that mediates the turnover of RNPs or their components, such
179 as autophagy.
180
181 To determine if autophagy was required for KapB-mediated PB disassembly, we first inhibited
182 autophagic flux by independently silencing two genes in the macroautophagy pathway, Atg5 and
183 Atg14 (Fig S2A, B). When either Atg5 or Atg14 were silenced in KapB-expressing HUVECs,
184 PBs were restored, whereas their silencing did not have the same effect in control cells (Fig 2A
185 and B). We then examined the ability of KapB to mediate PB disassembly in Atg5 -/- mouse
186 embryonic fibroblasts (MEFs), which (77) lack conversion of LC3-I to LC3-II (Fig S2C). KapB
187 failed to disassemble PBs in Atg5 -/- MEFs but did disassemble PBs in matched wild-type
188 controls (Fig S2D). Moreover, KapB expression resulted in a significant increase in Atg5 protein
189 levels in HUVECs (Fig S2A), consistent with our other data that show that KapB promotes
190 autophagy. Additionally, blocking autophagic degradation with BafA1 also restored PBs in
191 KapB-expressing cells (Fig 2C). Together, these data indicate that KapB mediates PB
192 disassembly by enhancing autophagy.
193
194 Autophagy, although always occurring at a basal level, can be upregulated by many different cell
195 stimuli including starvation or inhibition of mTOR using Torin-1, hereafter referred to as Torin
196 (78). It was previously reported that rapamycin, an inhibitor of mTORC1, caused a loss of PBs in
197 mammary epithelial cells (79). We reasoned that if we inhibited both mTOR complexes
198 mTORC1 and mTORC2 using Torin (80) to induce autophagy, PBs would disassemble. We
199 observed that the number of Hedls/Edc4 puncta were significantly reduced after Torin treatment,
200 indicating that chemical induction of autophagy also resulted in the disappearance of PBs (Fig

201 3A). To ensure that Torin treatment was inducing disassembly of PBs and not preventing
202 assembly, HUVECs were treated with sodium arsenite to induce PB formation; like KapB, Torin
203 treatment did not prevent the assembly of PBs under these conditions (Fig 3B).

204 Given these similarities, we wondered if KapB induced autophagy via inhibition of mTOR
205 complexes mTORC1 and mTORC2. To test this, we performed immunoblotting for the
206 phosphorylated form of the ribosomal protein S6 (Serine 235/236) (81) and the phosphorylated
207 forms of the Unc-51 like autophagy activating kinase (ULK1; Serine 757/555) component of the
208 ULK autophagy initiation complex, both of which are dephosphorylated when mTOR activity is
209 inhibited by Torin (82,83). Unlike Torin, KapB expression did not decrease phosphorylation of
210 S6 (Fig 3C) or ULK (Fig 3D). We also expressed a constitutively active form of MK2 in which
211 two threonine residues that are normally phosphorylated by the upstream kinase p38, have been
212 substituted with glutamic acid residues (T205E/T317E, called MK2EE) (84–86) and determined
213 the effect on phospho-S6 and phospho-ULK. We previously demonstrated that MK2EE caused
214 PB disassembly (52) and others showed it increased autophagic flux after starvation (69). Like
215 KapB, MK2EE expression did not decrease phosphorylation of S6 (Fig 3C) or ULK (Fig 3D).
216 These data indicate KapB does not inhibit mTOR activity to induce autophagy. Since KapB can
217 bind and activate MK2, we next wondered if KapB expression would mediate phosphorylation of
218 Beclin 1 at Serine 90, as shown by others for MK2EE (68). Like MK2EE, KapB induced
219 phosphorylation of Beclin 1 at Serine 90 (Fig 3E), indicating that induction of autophagy via
220 KapB expression is mediated by activation of Beclin 1. Taken together, these data show that
221 although both KapB expression and Torin treatment caused PB disassembly in an autophagy-
222 dependent manner, the mechanism used to upregulate autophagic flux differed in each case.

223 **Canonical autophagy is required for KapB-mediated increases in ARE-containing cytokine**
224 **transcripts**
225 PBs are nodes of post-transcriptional mRNA regulation and microscopically visible PBs are
226 associated with ARE-mRNA decay or suppression (43,51,52,54,55,87,88). However, in
227 untreated HUVECs, the transcription of most ARE-mRNAs is minimal. To activate transcription
228 of ARE-containing cytokines in a biologically relevant manner, rather than using common
229 inflammatory stimuli such as the bacterial product, lipopolysaccharide, we treated KapB-
230 expressing or control HUVECs with 0.22 μm-filtered conditioned media from KSHV latently
231 infected cells. Conditioned media from latent KSHV cells would be expected to contain
232 inflammatory cytokines, e.g. TNF, that are elevated in KS, without containing virions (89). We
233 then examined levels of some endogenous ARE-containing RNA transcripts in KapB-expressing
234 cells (Fig 4A). We observed significant increases of cytokine mRNA for IL-6 and IL-1β in
235 KapB-expressing cells compared to equivalently treated controls, suggesting these increases
236 resulted from reduced transcript decay in PBs (Fig 4A). In addition, treatment with Torin
237 promoted the enhanced steady-state levels of IL-1β and COX-2 (Fig 4B), suggesting that
238 inducing autophagy reduced the decay of some ARE-mRNA transcripts. To support these
239 findings and to simplify further studies, we utilized a luciferase reporter assay that we developed,
240 described in (66). Using this assay, we previously showed that KapB-mediated PB loss
241 correlated with enhanced luminescence of an ARE-containing firefly luciferase (FLuc) reporter
242 because its rapid turnover was reversed and FLuc translation was enhanced (52,66). Briefly,
243 HeLa cells were co-transfected with a FLuc construct containing the destabilizing AU-rich
244 element from the *CSF2* gene in its 3'UTR and a Renilla luciferase (RLuc) construct with no
245 ARE; transcription of both reporter constructs was then stopped by the addition of doxycycline.

246 In control (vector transfected) cells, the FLuc-ARE mRNA decayed rapidly and FLuc
247 luminescence relative to the RLuc transfection control was low. Torin treatment caused a
248 significant increase in FLuc/RLuc relative luminescence compared to DMSO-treated control
249 cells, supporting our RT-qPCR findings (Fig 4C) and suggesting that enhanced autophagy
250 reverses the constitutive turnover/suppression of the ARE-mRNA reporter. Furthermore, KapB
251 expression also caused a significant increase in FLuc/RLuc relative luminescence compared to
252 empty vector control cells (Fig 4D) as previously shown in (52). When canonical autophagy was
253 perturbed by either Atg5 or Atg14 silencing (Fig S3A, B) KapB-expressing cells displayed
254 significantly decreased luminescence compared to KapB-expressing controls (Figs 4D, E).
255 Likewise, when KapB-expressing cells were treated with BafA1, relative luminescence was
256 significantly decreased compared to KapB-expressing untreated control cells (Fig 4F). Together,
257 these data showed that canonical autophagy is required for KapB-mediated increases in cytokine
258 mRNA levels and the enhanced expression of an ARE-mRNA reporter.
259
260 **Dcp1a protein levels are decreased by KapB and Torin treatment**
261 Both KapB and Torin mediated PB disassembly but did not prevent *de novo* PB formation. We
262 reasoned that KapB and Torin could have this effect because they cause the autophagic
263 degradation of the entire PB granule. Alternatively, since some PB proteins have important
264 scaffolding roles that hold granules together (EDC4/Hedls, Xrn1, DDX6/Rck, Pat1b or Dcp1a
265 (90)), PB disassembly could be induced by KapB or Torin if one or more key PB proteins was
266 missing due to accelerated degradation. To differentiate between these two scenarios, we
267 immunoblotted for PB proteins after Torin treatment and in the context of KapB expression (Fig
268 5). Immunoblotting revealed that steady-state levels of Dcp1a were reduced in Torin-treated (Fig

269 5A) and KapB-expressing cells (Fig 5B); however, steady-state levels of the other PB-resident
270 proteins we tested were not affected (Fig 5A, C). Moreover, KapB-mediated Dcp1a decreases
271 were reversed by BafA1 treatment (Fig 5B) and steady-state levels of the SAR, p62, included as
272 a measure of autophagic flux, were likewise restored (Fig 5B). Together, these data suggest that
273 autophagy induction with Torin or KapB expression promote the accelerated degradation of the
274 PB-resident protein Dcp1a, but not all PB proteins. Silencing the canonical autophagy gene,
275 *Atg5*, resulted in a reversal of KapB-mediated Dcp1a loss (Fig 5D), suggesting that autophagy is
276 required for the loss of Dcp1a observed in KapB-expressing cells.
277
278 **KapB-mediated PB disassembly and ARE-mRNA stabilization require the selective**
279 **autophagy receptor NDP52**
280 After establishing a link between KapB expression, autophagy, and PB disassembly, we
281 wondered what specific autophagy mechanisms were at work and if selective autophagy
282 receptors (SARs) were involved. One previous study observed the SAR, NDP52, partially co-
283 localized with some PB proteins (91). For this reason, we used RNA silencing to investigate
284 whether NDP52, p62, VCP, NBR1, or OPTN were required for KapB-mediated PB disassembly.
285 Despite trying several different shRNA sequences, our attempts to silence NBR1 were
286 unsuccessful, and shRNAs targeting VCP resulted in significant HUVEC toxicity (Fig S4A, B).
287 Therefore, the role of these molecules in KapB-mediated PB disassembly could not be
288 determined. Knockdown of NDP52, p62, and OPTN was validated in control and KapB-
289 expressing cells (Fig S4C-E). Silencing of p62 or OPTN did not restore PBs in KapB-expressing
290 cells whereas NDP52 knockdown significantly restored PBs (Fig 6A, Fig S4F). These data
291 pinpointed an important role for NDP52 and selective autophagy in KapB-mediated PB

292 disassembly. We then tested whether NDP52 silencing could prevent Torin-mediated PB
293 disassembly and found that PBs could not be disassembled in cells lacking NDP52 (Fig 6B,
294 S4G). Since steady-state levels of the decapping cofactor, Dcp1a, decreased in response to KapB
295 infection and Torin treatment (Fig 5), we examined the steady-state level of Dcp1a after Torin
296 with and without NDP52 silencing (Fig 6C). Although Dcp1a was significantly diminished after
297 Torin treatment, NDP52 silencing did not restore Dcp1a to control levels. We decided to
298 consider another PB protein, Pat1b, a decapping cofactor known to interact with several other PB
299 proteins including Dcp1a, DDX6, and Hedls, suggesting that Pat1b is an important scaffold for
300 PB components (44). Immunoblotting revealed that Torin treatment significantly diminished
301 steady-state levels of Pat1b, and that this decrease was restored to control levels when Torin
302 treatment was performed in NDP52-silenced cells (Fig 6C). These data suggest that levels of the
303 PB component proteins Pat1b, and to a lesser extent, Dcp1a, are regulated by NDP52-dependent
304 autophagic degradation.
305
306 We also examined whether these SARs were required for KapB-enhanced relative luminescence
307 in our ARE-mRNA reporter assay. We validated silencing of NDP52, p62, and OPTN in HeLa
308 cells (Fig S5A-C). We found that p62 or OPTN knockdown had no effect on KapB-mediated
309 ARE-containing reporter luminescence, but NDP52 silencing decreased the signal compared to
310 non-targeting, KapB-expressing controls (Fig 6D), further supporting the role of NDP52 in
311 autophagy-mediated PB disassembly. We then performed an NDP52 complementation
312 experiment. We first silenced endogenous NDP52 in control or KapB-expressing HUVECs using
313 shRNAs targeting the 3'UTR of NDP52 and verified its knockdown (Fig S6A). Next, NDP52
314 expression was restored by overexpressing a fluorescently tagged NDP52 construct.

315 Complementation of NDP52-silenced HUVECs with NDP52 restored KapB-mediated PB
316 disassembly compared to vector controls (Fig 6E-F; S6B, C). Notably, complementation with
317 NDP52 in control cells that lacked KapB failed to induce PB disassembly, suggesting that KapB-
318 or Torin-mediated autophagy increase is an important component of the PB disassembly
319 phenotype. Taken together, these data indicate that NDP52 is required for KapB- and Torin-
320 mediated PB disassembly and KapB-mediated ARE-mRNA stabilization.
321
322 **Atg5 and NDP52 are required for KSHV-mediated PB disassembly**
323 Autophagy regulation during KSHV latency is complex, as the viral gene products v-FLIP and v-
324 cyclin also modulate autophagic flux in addition to KapB (35,36). To simplify our study of
325 autophagy and PBs, we initially used a reductionist approach, expressing only KapB in
326 HUVECs. However, to confirm the relevance of our study to KSHV infection, we performed a
327 study in KSHV-infected HUVECs. We infected HUVECs with rKSHV.219 (92) for 96 hours to
328 permit latency establishment and then treated or with either BafA1 or a vehicle control for 30
329 minutes prior to staining infected cells for LC3 puncta as a measure of autophagic flux. We
330 observed a dramatic increase in LC3 puncta in KSHV infected cells after BafA1 treatment when
331 compared to mock infection controls (Fig 7A). These data demonstrate that autophagic flux was
332 upregulated during KSHV latency despite the concurrent expression of vFLIP, an inhibitor of
333 autophagy, during this infection phase.(35). In parallel, we immunoblotted infected cell lysates
334 and observed that KSHV increased phosphorylation of Ser90 of Beclin 1 (Fig 7B), consistent
335 with earlier observations of Ser90 phosphorylation after ectopic expression of KapB (Fig 3D).
336 To confirm if KapB was necessary for upregulated autophagic flux after KSHV infection, we
337 used a recombinant KSHV that does not express KapB (delB BAC16) and matched wild-type

338 control (BAC16 KSHV), described in our recent publication (93). We infected HUVECs with
339 WT BAC16 KSHV or delB BAC16 virus for 96 hours to permit latency establishment. WT
340 BAC16 KSHV latency also induced LC3 puncta formation and phosphorylation of Ser90 of
341 Beclin 1, consistent with our result using the KSHV.219 virus, whereas infection with delB
342 BAC16 virus failed to enhance autophagic flux or phosphorylation of Beclin 1 at Ser90 (Fig 7C,
343 D). We confirmed these data in iSLKs, a KSHV producer cell line known for tight control over
344 latency (92). Naïve iSLKs were infected with WT BAC16 KSHV or delB BAC16 virus for one
345 week to permit latency establishment, and LC3-II accumulation in the presence of BafA1
346 treatment was determined by immunoblotting (Fig 7E). LC3-II showed higher accumulation after
347 BafA1 treatment in WT KSHV-infected iSLK cells than those infected with delB BAC16 virus
348 (Fig 7E), confirming that autophagic flux was enhanced in a KapB-dependent manner during
349 KSHV latent infection of iSLK cells. Together, these data validate a necessary role for KapB in
350 KSHV enhancement of autophagic flux and show that during this KSHV infection phase,
351 autophagy proceeds via a non-canonical activation mechanism that involves the phosphorylation
352 of Ser90 in Beclin 1 (69).
353
354 In our previous work, we showed that KSHV infection induced PB disassembly (52) and more
355 recently we confirmed that KapB was not only sufficient but also necessary for this effect with
356 the delB BAC16 virus (93) . To determine if autophagic machinery is also required for PB
357 disassembly in the context of KSHV infection, we silenced *Atg5* or *NDP52* in HUVECs prior to
358 infecting with rKSHV.219 for 96 hours to establish latency, then stained for PBs. Consistent
359 with our data that showed a requirement for autophagy in KapB-mediated PB disassembly,
360 blocking autophagic degradation by silencing *Atg5* or *NDP52* restored PBs in KSHV-infected

361 cells (Fig 8A-B). We quantified PBs and compared their levels between KSHV-infected and
362 mock-infected cells in control cells or in silenced cells. We did not compare PB counts between
363 KSHV-infected and silenced cells to infected controls because silencing of autophagy regulatory
364 proteins influences PB homeostasis. In control cells that expressed a non-targeting shRNA,
365 KSHV infection decreased PBs, as expected from our previous work (Fig 8A). However, when
366 either *Atg5* or *NDP52* were silenced, KSHV infection had no effect on PBs relative to the
367 matched uninfected control, and silencing autophagy regulatory proteins restored PBs to levels
368 observed in the absence of infection (Fig 8A). These data confirm an essential role for autophagy
369 and the selective autophagy receptor NDP52 in KSHV-mediated PB disassembly.
370
371 To understand more about the molecular mechanism of NDP52-dependent PB disassembly
372 during KSHV infection, we first immunoblotted for steady-state levels of NDP52. KSHV
373 infection did not significantly alter the amount of NDP52 protein (Fig 8C). We speculated that
374 rather than influencing NDP52 production, enhanced autophagic flux observed after KapB
375 expression, KSHV infection, or Torin, would enhance the interaction of NDP52 with its target
376 cargo. As Torin treatment decreased Dcp1a and Pat1b protein levels, and Pat1b was restored by
377 NDP52 silencing (Fig 3), we tested if either Dcp1a or Pat1b were NDP52 interacting partners.
378 To determine this, we overexpressed FLAG-tagged NDP52 with GFP-tagged Dcp1a, GFP-
379 tagged Pat1b or a GFP control and immunoprecipitated using a FLAG antibody. We verified
380 immunoprecipitation of NDP52 and that we could detect the expression of GFP and GFP-tagged
381 Dcp1a in whole cell lysate; however, neither GFP alone nor GFP-Dcp1a co-immunoprecipitated
382 with NDP52 (Fig 8D). By contrast, we did co-immunoprecipitate GFP-Pat1b with FLAG-
383 NDP52. These data suggest that NDP52 and Pat1b interact which could result in delivery of

384 Pat1b and possibly other PB components to the nascent autophagosome for degradation. We
385 reasoned that if NDP52 and Pat1b interact, KSHV-mediated autophagy should decrease steady-
386 state levels of Pat1b. Consistent with this, Pat1b protein levels were significantly decreased after
387 KSHV infection (Fig 8E). KSHV infection also decreased the steady-state levels of Dcp1a, a
388 result consistent with earlier data that showed Dcp1a decreased in response to KapB expression
389 and Torin treatment. From these data, we propose the following model: KSHV infection or KapB
390 expression enhances autophagic flux via Beclin phosphorylation while Torin dephosphorylates
391 the ULK complex. In both cases, elevated autophagic flux increases the delivery of Pat1b, and
392 perhaps other PB components that interact with Pat1b (such as Dcp1a), to nascent
393 autophagosomes via recognition of Pat1b by the selective autophagy receptor, NDP52. This
394 interaction decreases the abundance of Pat1b, a PB scaffolding protein, resulting in PB
395 disassembly (Fig 8F).
396

397
398 **Discussion**

399 Here, we demonstrated that the KSHV protein KapB relies on selective autophagy to cause PB
400 disassembly and enhance ARE-mRNA stability. Furthermore, we identified NDP52 as the
401 selective autophagy receptor required for this process. To our knowledge, this is the first report
402 that provides a molecular basis for NDP52-mediated turnover of endogenous PBs and the first
403 description of the contribution of NDP52 to immune regulation by altering inflammatory
404 cytokine RNA turnover/suppression in PBs. We showed that PB disassembly induced by
405 infection with KSHV required Atg5 and NDP52, suggesting an important role for KapB-
406 mediated elevated autophagic flux and PB catabolism in regulating KSHV-associated
407 inflammation. Our major findings are: i) KapB and KSHV latent infection increased autophagic
408 flux by phosphorylation of the autophagy regulatory protein, Beclin 1, thereby contributing to
409 the complex regulation of autophagic processes during KSHV latent infection and
410 tumourigenesis, ii) KapB expression was necessary for KSHV-mediated autophagy increases
411 during latent infection, iii) KapB- and KSHV-mediated PB disassembly and enhanced translation
412 of an ARE-containing reporter required canonical autophagy machinery and the selective
413 autophagy receptor, NDP52, iv) Activation of autophagy by chemical inhibition of mTORC1
414 using Torin caused PB disassembly using a mechanism that was dependent on canonical
415 autophagy and NDP52, suggesting that KapB manipulates an existing cellular pathway that
416 regulates PB catabolism. These results reveal that PB turnover elicited by the KSHV KapB
417 protein during infection requires a host pathway that uses NDP52 to enhance PB catabolism and
418 promote inflammatory molecule production.
419

420 MK2 activation promotes autophagy by phosphorylating Beclin 1 (69); therefore, we
421 hypothesized that KapB, an MK2-activating viral protein (68), would utilize autophagy to
422 promote PB clearance. Our data showed that both KapB and MK2EE increased autophagic flux
423 via phosphorylation of Beclin 1 at Serine 90 and that KapB-mediated PB disassembly required
424 the canonical autophagy proteins Atg5 and Atg14, and the selective autophagy protein NDP52.
425 Our data are supported by previous work showing that in yeast, PB recycling requires canonical
426 autophagy machinery, and in mammalian cells NDP52 colocalizes with a GFP-tagged version of
427 Dcp1a when overexpressed (91,94). We add significantly to these studies, by performing our
428 work in primary human endothelial cells and by staining for endogenous PBs using
429 immunofluorescence for the decapping co-factor Hedls/EDC4. We revealed that when KapB was
430 expressed, endogenous PBs disassemble via an Atg5-, Atg14-, and NDP52-dependent
431 mechanism. We also complemented NDP52-silenced cells with an shRNA-resistant NDP52 and
432 observed the restoration of KapB-mediated PB disassembly. This occurred only in cells that
433 expressed KapB and not in control cells that overexpressed NDP52, an observation that suggests
434 that KapB-mediated autophagy increases are required for NDP52-mediated PB disassembly.
435 These data also suggest that NDP52 is required to select the PB protein cargo for autophagic
436 degradation and this is required for KSHV and KapB-mediated PB disassembly, akin to that
437 observed in other studies on NDP52 SAR function (95,96). Consistent with this, we showed that
438 the PB scaffolding protein, Pat1b, co-immunoprecipitated with NDP52, providing a molecular
439 basis for this interaction. In addition to identifying cargo for clearance, NDP52 has recently been
440 shown to orchestrate autophagosome biogenesis by recruiting essential autophagic machinery to
441 initiation sites (14,97,98), suggesting another possible way that NDP52 may promote KapB-
442 mediated PB disassembly.

443

444 Immunoelectron microscopy showed that PBs range in size from 150 to 350 nm and possess an
445 external area of peripheral protrusions that contain the helicase Rck/DDX6 anchored to a dense
446 central core of decay enzymes, including Dcp1a and Xrn1 (38). Many PB-localized enzymes are
447 required for PB stability including Dcp1a and Pat1b; however, only three PB proteins are
448 required for *de novo* PB formation, DDX6, the translation suppressor, 4E-T, and LSM14a
449 (44,90). Our data showed that KapB expression decreased the steady-state levels of Dcp1a, while
450 the steady-state levels of other PB proteins were unaffected. Inducing autophagy with the
451 mTORC1/2 inhibitor Torin also decreased steady-state levels of Dcp1a and Pat1b, but not other
452 PB proteins; however only Pat1b protein levels were restored to control levels when NDP52 was
453 silenced. These data support a model where the entire PB granule is not degraded by autophagy,
454 but PB disassembly is induced by the selective degradation of NDP52-bound Pat1b with or
455 without the Pat1b-interacting protein, Dcp1a. Consistent with this, we show that PBs can still
456 form during KapB expression if we overexpress Dcp1a-GFP or block translation using sodium
457 arsenite. Dcp1a is a target for other viruses that mediate PB disassembly; for example, infection
458 with poliovirus caused PB disassembly and the loss of Dcp1a over a time course of infection
459 (99); adenovirus infection has been shown to re-localize Pat1b from PBs to cytoplasmic
460 aggresomes during infection (100). We do not yet understand if KSHV infection or Torin
461 treatment alters Pat1b to promote its interaction with NDP52 and subsequent autophagic
462 degradation and PB disassembly; however, we speculate that post-translational modifications of
463 Pat1b and perhaps Dcp1a may be involved (101–107).

464

465 Infection with KSHV induces high levels of pro-inflammatory cytokines, chemokines and
466 angiogenic factors such as TNF, IL-1α, IL-1β, IL-6, CXCL8, IFN-γ, VEGF, COX-2 and GM-
467 CSF (56–62). Although several KSHV proteins promote the transcription of these products,
468 many harbor AREs in the 3'UTR of their cognate mRNA, meaning their transcripts are subject to
469 additional post-transcriptional regulation by PBs. We previously showed that KapB and the lytic
470 KSHV protein, viral G-protein-coupled receptor (vGPCR) enhanced the translation of an ARE-
471 containing reporter and elevated steady-state levels of inflammatory products, and that this
472 coincided with the ability of KapB and vGPCR to induce PB disassembly (51,52,66,68). We now
473 show that KapB expression increased steady-state levels of three ARE-containing transcripts, IL-
474 6, GM-CSF, and TNF, coincident with PB disassembly. However, KapB expression did not
475 increase CXCL8, indicating that there remains additional regulation, beyond PB disassembly, of
476 ARE-mRNA decay (108,109). We also show that the ability of KapB to induce PB disassembly
477 and enhance our ARE-mRNA reporter requires both canonical and selective autophagic
478 machinery. RNA transcripts for some canonical autophagy proteins in the Atg5-Atg12-Atg16
479 complex are also rendered labile by 3'UTR AREs, suggesting that expression of KapB or
480 vGPCR may cause a pro-autophagic positive feedback loop where PB disassembly culminates in
481 the enhanced translation of pro-autophagic products (110,111), a feature that may be aided
482 further by KapB-mediated upregulation of the ARE-mRNA stabilizing RBP, HuR (112). This
483 feed forward loop may contribute to the KapB-mediated increase in Atg5 protein levels and the
484 induction of autophagic flux. Taken together, our study reveals a novel way that KSHV infection
485 manipulates autophagic machinery to induce PB turnover and promote inflammatory molecule
486 production. The fact that KSHV encodes more than one protein that reverses the constitutive
487 repression of inflammatory mRNAs in PBs highlights its central importance.

488

489 Viral gene products both enhance and block autophagic flux during latent KSHV infection; v-
490 cyclin induces oncogene-induced senescence via induction of autophagy, whereas v-FLIP
491 counteracts v-cyclin, blocking autophagy by binding Atg3 and inhibiting LC3 lipidation (35,36).
492 We show herein that KapB also upregulates autophagic flux, and that KapB is necessary for the
493 enhanced autophagic flux we observe after KSHV infection of ECs. These data are consistent
494 with autophagy enhancement observed in latent B-lymphocytes (BCBL-1 cells) (113) and show
495 for the first time that KSHV latent infection of primary ECs culminates in an elevated autophagic
496 state. It is possible that KSHV products may cooperate to promote autophagy during latency,
497 perhaps via dysregulation of the cellular transcription factor, Nrf2, responsible for the activation
498 of several antioxidant response genes as well as NDP52 (114–116). Nrf2 activity is upregulated
499 by the viral protein vFLIP after *de novo* infection of ECs and during KSHV latency (117,118).
500

501 In viral cancers like KS, autophagic flux promotes a pro-tumourigenic and pro-inflammatory
502 environment (113,119–121). The data shown herein brings new understanding to this complex
503 relationship during KSHV infection. We show that KapB was both sufficient to induce
504 autophagic flux and was necessary for enhanced autophagy during KSHV latent infection. We
505 confirmed that autophagy machinery and NDP52 were required for PB disassembly; this
506 supports an important role for KapB in eliciting the pro-inflammatory environment associated
507 with latent KSHV infection and KS. The manipulation of NDP52 function and autophagic flux
508 by KSHV and KapB is yet another example of the ingenuity with which viruses usurp cellular
509 processes; revealing a regulatory network that links NDP52 to inflammatory molecule
510 production via PB catabolism.

511

512 **Materials and Methods**

513 **Cell culture**

514 All cells were grown at 37 °C with 5% CO_2 and 20% O_2. HEK293T cells (ATCC), HeLa Tet-Off
515 cells (Clontech), Atg5 +/+ and -/- MEFs (122), HeLa Flp-In TREx GFP-Dcp1a cells (a generous
516 gift from Anne-Claude Gingras), and iSLK.219 cells (a generous gift from Don Ganem) (92)
517 were cultured in DMEM (Thermo Fisher) supplemented with 100 U/mL penicillin, 100 µg/mL
518 streptomycin, 2 mM L-glutamine (Thermo Fisher) and 10% FBS (Thermo Fisher). iSLK.219
519 cells were additionally cultured in the presence of puromycin (10 µg/mL). HUVECs (Lonza)
520 were cultured in endothelial cell growth medium (EGM-2) (Lonza). HUVECs were seeded onto
521 gelatin (1% w/v in PBS)-coated tissue culture plates or glass coverslips. All drug treatments were
522 performed for the times indicated in each experiment at the concentrations listed in Table 1.

523 **Cloning**

524 All plasmids used in this study can be found in Table 2. All shRNAs were generated by cloning
525 shRNA hairpin sequences found in Table 3 into pLKO.1-TRC Puro,pLKO.1-TRC cloning vector
526 was a gift from David Root (Addgene plasmid # 10878; http://n2t.net/addgene:10878;
527 RRID:Addgene_10878) or pLKO.1-blast, pLKO.1-blast was a gift from Keith Mostov (Addgene
528 plasmid #26655; http://n2t.net/addgene:26655; RRID:Addgene_26655). pcDNA-FLAG-NDP52
529 was made by amplifying NDP52 from RFP-NDP52 (a generous gift from Dr. Andreas Till) using
530 the primers found in Table 4 and performing a restriction digest with EcoRI and BamHI to insert
531 into FLAG-HA-pCDNA, FLAG-HA-pcDNA3.1 was a gift from Adam Antebi (Addgene
532 plasmid # 52535; http://n2t.net/addgene:52535; RRID:Addgene_52535). pLJM1-GFP-Dcp1a
533 was generated from pT7-EGFP-C1-HsDcp1a, pT7-EGFP-C1-HsDCP1a was a gift from Elisa
534 Izaurralde (Addgene plasmid # 25030; http://n2t.net/addgene:25030; RRID:Addgene_25030)

535 through restriction digest with AgeI and EcoRI to insert into pLJM1. pLJM1-GFP-Pat1b was
536 generated from Pat1b-GFP (a generous gift from Dr. Nancy Standart) through restriction digest
537 with NheI and BamHI to insert into pLJM1.

538 **Lentivirus Production and Transduction**

539 All lentiviruses were generated using a second-generation system. Briefly, HEK293T cells were
540 transfected with pSPAX2, MD2G, and the plasmid containing a gene of interest or hairpin using
541 polyethylimine (PEI, Polysciences). psPAX2 was a gift from Didier Trono (Addgene plasmid
542 #12260; http://n2t.net/addgene:12260; RRID:Addgene_12260) and pMD2.G was a gift from
543 Didier Trono (Addgene plasmid #12259; http://n2t.net/addgene:12259; RRID:Addgene_12259).
544
545 Viral supernatants were harvested 48 h post-transfection, clarified using a 0.45 µ
546 polyethersulfone filter (VWR), and frozen at -80°C until use. For transduction, lentiviruses were
547 thawed at 37°C and added to target cells in complete media containing 5 µg/mL polybrene
548 (Sigma) for 24 h. The media was changed to selection media containing 1 µg/mL puromycin or 5
549 µg/mL blasticidin (Thermo) and cells were selected for 48 h before proceeding with
550 experiments.

551 **Viral conditioned media treatments**

552 iSLK.219 cells (latently infected with rKSHV.219 virus) were sub-cultured into a 10 cm cell
553 culture dish and grown without puromycin for 72 h. At 72 h, conditioned media was reserved
554 and cleared of cellular debris by centrifugation at 500 G for 5 min. Supernatant was collected
555 and filtered through a 0.22 µM polyethersulfone (PES) membrane filter (VWR) and stored in
556 aliquots at -80. Prior to the experiment, conditioned media was thawed at 37°C and combined

557 1:1 with fresh HUVEC EGM-2 media and used to treat vector or KapB-expressing HUVECs for
558 0 or 6 h prior to total RNA harvest.

559 **Production of KSHV**

560 Cloning and creation of the iSLK-BAC16ΔKapB cell line is described in (93). iSLK.219 or
561 iSLK-BAC16 cells were sub-cultured into a 10 cm cell culture dish without puromycin and
562 reactivated from latency with either 1 µg/mL doxycycline (Sigma-Aldrich) alone (iSLK.219) and
563 1 µg/mL doxycycline and 1 mM sodium butyrate (Sigma-Aldrich) (iSLK-BAC16). After 72 h,
564 supernatants were collected, centrifuged to remove cellular debris, aliquoted, and stored at -80°C
565 until use.

566 **KSHV infection**

567 Sub-confluent (50-70%) 12-well or 6-well plates of HUVECs or naïve iSLKs (92), respectively,
568 were incubated with either rKSHV.219 or KSHV BAC16 viral inoculum diluted in antibiotic and
569 serum free DMEM containing 5 µg/mL polybrene. Plates were centrifuged at 800 x *g* for 2 hours
570 at room temperature (123), the inoculum was removed and replaced with either EGM-2. For
571 KSHV BAC16 infections, WT and ΔKapB inoculums were normalized empirically prior to
572 infection to circumvent our previously observed impairment in latency establishment during
573 ΔKapB infection (93). To establish robust and stable latency in Figure 7, *de novo* infected iSLKs
574 were expanded from a 6-well to a 10cm dish, selected with 500 µg/mL hygromycin B
575 (ThermoFisher), split once, then selected with 1200 µg/mL hygromycin B for a combined period
576 of one week prior to seeding.

577 **Immunofluorescence**

578 Cells were seeded onto coverslips for immunofluorescence experiments and fixed for 10 mins at
579 37 °C in 4% (v/v) paraformaldehyde (Electron Microscopy Sciences). Samples were

580 permeabilized with 0.1% (v/v) Triton X-100 (Sigma-Aldrich) for 10 min at room temperature
581 and blocked in 1% human AB serum (Sigma-Aldrich) for 1 h at room temperature. For
582 autophagosome immunofluorescence cells were fixed for 10 min in ice cold methanol at -20 °C
583 and blocked in 1% human AB serum for 1 h at room temperature. Primary and secondary
584 antibodies were diluted in 1% human AB serum and used at the concentrations in Table 5.
585 Samples were mounted with Prolong Gold AntiFade mounting media (Thermo). Image analysis
586 was performed using CellProfiler (cellprofiler.org), an open source platform for image analysis
587 (Carpenter et al., 2006); quantification of puncta was performed as previously described, with the
588 exception that cells were defined by propagating out a set number of pixels from each nucleus
589 (124).

590 **Co-Immunoprecipitation**

591 HEK293T cells were transfected with plasmids expressing either FLAG-HA-pCDNA (empty
592 vector) or pcDNA-FLAG-NDP52 with either pLJM1-GFP (control), pLJM1-GFP-Dcp1a, or
593 pLJM1-GFP-Pat1b for 48 h. Cells were harvested in lysis buffer (150 mM NaCl, 10 mM Tris pH
594 7.4, 1 mM EDTA, 1% v/v Triton X-100, 0.5% v/v NP-40, Roche protease inhibitor tablet) and
595 incubated with a FLAG mouse antibody (CST) overnight at 4 °C. Protein G magnetic beads
596 (Biorad) were incubated overnight at 4 °C with 5 mg/mL BSA in lysis buffer without Triton X-
597 100 or NP-40. Immunoprecipitation was performed and samples were eluted from the magnetic
598 beads through boiling in 4x Laemmli buffer (Biorad) with 10% v/v beta-mercaptoethanol.
599

600 **Immunoblotting**

601 Cells were lysed in 2x Laemmli buffer and stored at -20°C until use. The DC Protein Assay
602 (Bio-Rad) was used to quantify protein concentration as per the manufacturer's instructions. 10-

603 15 µg of protein lysate was resolved by SDS-PAGE on TGX Stain-Free acrylamide gels
604 (BioRad). Total protein images were acquired from the PVDF membranes after transfer on the
605 ChemiDoc Touch Imaging system (BioRad). Membranes were blocked in 5% bovine serum
606 albumin (BSA) or skim milk in Tris-buffered saline-Tween20 (TBS-T). Primary and secondary
607 antibodies were diluted in 2.5% BSA or skim milk, dilutions can be found in Table 5.
608 Membranes were visualized using Clarity Western ECL substrate and the ChemiDoc Touch
609 Imaging system (BioRad).

610 **Luciferase Assays**

611 Luciferase assays were performed as previously described (66). HeLa Tet-Off cells were
612 transduced with recombinant lentivirus expressing different shRNAs and selected. Cells were
613 transfected according to Corcoran *et al.* (2011) with pTRE2 Firefly Luciferase ARE (FLuc),
614 pTRE2 Renilla Luciferase (RLuc), and the expression plasmid of interest using Fugene HD
615 (Promega). FLuc and RLuc activity were quantified using the Dual Luciferase Assay Kit
616 (Promega) and read on a GloMax multi-detection system (Promega).

617 **Quantitative PCR**

618 RNA was collected using a RNeasy Plus Mini Kit (Qiagen) according to the manufacturer's
619 instructions and stored at -80°C until further use. RNA concentration was determined and was
620 reverse transcribed using Maxima H Minus First Strand cDNA Synthesis Kit (Thermo Fisher)
621 using a combination of random and oligo (dT) primers according to the manufacturer's
622 instructions. cDNA was diluted either 1:5 or 1:10 for all qPCR experiments and GoTaq qPCR
623 Master Mix (Promega) was used to amplify cDNA. The ΔΔquantitation cycle (Cq) method was
624 used to determine the fold change in expression of target transcripts. qPCR primer sequences can
625 be found in Table 6.

626 **Statistics**

627 Data shown are the mean ± standard error of the mean (SEM). Statistical significance was
628 determined using a one-way ANOVA, a 2-way ANOVA or Student's t-test when appropriate
629 with the applicable post-test (indicated in the corresponding figure legends). All statistics were
630 performed using GraphPad Prism v.9.0.

631

632 **Acknowledgements**

633 The authors would like to dedicate this manuscript to Dr. Beth Levine, who was a leader in the
634 field of autophagy and viruses and who inspired this work. We sincerely thank the members of
635 the Corcoran lab for helpful discussions. We would like to thank Dr. Craig McCormick
636 (Dalhousie University), Dr. Eric Pringle (Dalhousie University), and Dr. Andrew Leidal (UCSF)
637 for valuable feedback on this manuscript and the McCormick lab for plasmids, expertise, and
638 advice. We would like to thank Mr. Stephen Whitefield and Ms. Mary Ann Trevors in the
639 Dalhousie *CORES* (Cellular and Molecular Digital Imaging and Electron Microscopy core
640 facilities) and Dr. Anne Vaahtokari of the Charbonneau Microscopy Facility, UCalgary for
641 microscopy support. We would like to thank Dr. Andreas Till (University of Bonn), Dr. Anne-
642 Claude Gingras (Lunenfeld-Tanenbaum Research Institute) and Dr. Don Ganem (Novartis) for
643 sharing valuable reagents. Model figure created with BioRender. GKS was supported by a CIHR
644 CGS-M scholarship and Scotia Scholars NSHRF graduate training award. ELC was supported by
645 a Killam predoctoral scholarship, an NSERC CGS-M scholarship, and a Nova Scotia Graduate
646 scholarship. MK was supported by a CSM graduate training award, a CIHR CGS-M scholarship,
647 and a CIHR doctoral award. Operating funds to support this work derive from a CIHR Project
648 Grant PJT-153210 to JAC.

Author Contributions

Carolyn-Ann Robinson: Conceptualization, Experimentation, Analysis, Paper Writing

Gillian K. Singh: Conceptualization, Experimentation, Analysis, Paper Writing

Mariel Kleer: Experimentation, Analysis, Paper Writing

Elizabeth L. Castle: Analysis

Bre Q. Boudreau: Experimentation

Jennifer A. Corcoran: Conceptualization, Experimentation, Supervision, Funding Acquisition, Project Administration, Paper Writing

Conflict of Interest

The authors have no competing interests to declare.

663 **References**

664

665 1. Dikic I, Elazar Z. Mechanism and medical implications of mammalian autophagy. Nat

666 Rev Mol Cell Biol. 2018;19:349–64.

667 2. Levine B, Kroemer G. Biological Functions of Autophagy Genes: A Disease Perspective.

668 Cell. 2019;176: 11-42.

669 3. Morishita H, Mizushima N. Diverse cellular roles of autophagy. Annu Rev Cell Dev Biol.

670 2019;35: 453–75.

671 4. Lawrence RE, Zoncu R. The lysosome as a cellular centre for signalling, metabolism and

672 quality control. Nat Cell Biol. 2019;21:133-142.

673 5. Beese CJ, Brynjólfsdóttir SH, Frankel LB. Selective Autophagy of the Protein

674 Homeostasis Machinery: Ribophagy, Proteaphagy and ER-Phagy. Front Cell Dev Biol.

675 2020;7: 373.

676 6. Johansen T, Lamark T. Selective Autophagy: ATG8 Family Proteins, LIR Motifs and

677 Cargo Receptors. J Mol Biol. 2020;432: 80-103.

678 7. Kirkin V, Rogov V V. A Diversity of Selective Autophagy Receptors Determines the

679 Specificity of the Autophagy Pathway. Mol Cell. 2019;76: 268-285.

680 8. Rogov V, Dötsch V, Johansen T, Kirkin V. Interactions between Autophagy Receptors

681 and Ubiquitin-like Proteins Form the Molecular Basis for Selective Autophagy. Mol Cell.

682 2014;53:167–78.

683 9. Tumbarello DA, Manna PT, Allen M, Bycroft M, Arden SD, Kendrick-Jones J, et al. The

684 Autophagy Receptor TAX1BP1 and the Molecular Motor Myosin VI Are Required for

685 Clearance of Salmonella Typhimurium by Autophagy. PLoS Pathog. 2015;11: e1005174.

686 10. Sarraf SA, Shah H V., Kanfer G, Pickrell AM, Holtzclaw LA, Ward ME, et al. Loss of

687 TAX1BP1-Directed Autophagy Results in Protein Aggregate Accumulation in the Brain.
688 Mol Cell. 2020;80: 779-785.
689 11. Khaminets A, Behl C, Dikic I. Ubiquitin-Dependent And Independent Signals In Selective
690 Autophagy. Trends Cell Biol. 2016;26: 6–16.
691 12. Rogov V V, Stolz A, Ravichandran AC, Rios-Szwed DO, Suzuki H, Kniss A, et al.
692 Structural and functional analysis of the GABARAP interaction motif (GIM). EMBO Rep.
693 2017;18: 1382-1396.
694 13. Marshall RS, Hua Z, Mali S, McLoughlin F, Vierstra RD. ATG8-Binding UIM Proteins
695 Define a New Class of Autophagy Adaptors and Receptors. Cell. 2019;177: 766-781.
696 14. Ravenhill BJ, Boyle KB, von Muhlinen N, Ellison CJ, Masson GR, Otten EG, et al. The
697 Cargo Receptor NDP52 Initiates Selective Autophagy by Recruiting the ULK Complex to
698 Cytosol-Invading Bacteria. Mol Cell. 2019;74: 320-329
699 15. Turco E, Witt M, Abert C, Bock-Bierbaum T, Su MY, Trapannone R, et al. How
700 RB1CC1/FIP200 claws its way to autophagic engulfment of SQSTM1/p62-ubiquitin
701 condensates. Autophagy. 2019;15: 1475-77.
702 16. Vargas JNS, Wang C, Bunker E, Hao L, Maric D, Schiavo G, et al. Spatiotemporal
703 Control of ULK1 Activation by NDP52 and TBK1 during Selective Autophagy. Mol Cell.
704 2019;74: 347-362.
705 17. Chen M, Meng Q, Qin Y, Liang P, Tan P, He L, et al. TRIM14 Inhibits cGAS
706 Degradation Mediated by Selective Autophagy Receptor p62 to Promote Innate Immune
707 Responses. Mol Cell. 2016;64(1):105–19.
708 18. Du Y, Duan T, Feng Y, Liu Q, Lin M, Cui J, et al. LRRC25 inhibits type I IFN signaling
709 by targeting ISG15-associated RIG-I for autophagic degradation. EMBO J.

710 2018;37(3):351–66.
711 19. Jin S, Tian S, Luo M, Xie W, Liu T, Duan T, et al. Tetherin Suppresses Type I Interferon
712 Signaling by Targeting MAVS for NDP52-Mediated Selective Autophagic Degradation in
713 Human Cells. Mol Cell. 2017;68:308-322.
714 20. Prabakaran T, Bodda C, Krapp C, Zhang B, Christensen MH, Sun C, et al. Attenuation of
715 c GAS - STING signaling is mediated by a p62/ SQSTM 1-dependent autophagy pathway
716 activated by TBK1. EMBO J. 2018;37: e97858.
717 21. Yang Q, Liu TT, Lin H, Zhang M, Wei J, Luo WW, et al. TRIM32-TAX1BP1-dependent
718 selective autophagic degradation of TRIF negatively regulates TLR3/4-mediated innate
719 immune responses. PLoS Pathog. 2017;13: e1006600.
720 22. He X, Zhu Y, Zhang Y, Geng Y, Gong J, Geng J, et al. RNF 34 functions in immunity
721 and selective mitophagy by targeting MAVS for autophagic degradation. EMBO J.
722 2019;38: e100978.
723 23. Seth RB, Sun L, Ea CK, Chen ZJ. Identification and characterization of MAVS, a
724 mitochondrial antiviral signaling protein that activates NF-κB and IRF3. Cell.
725 2005;122:669–82.
726 24. Wu Y, Jin S, Liu Q, Zhang Y, Ma L, Zhao Z, et al. Selective autophagy controls the
727 stability of transcription factor IRF3 to balance type I interferon production and immune
728 suppression. Autophagy. 2020;17: 1376-92
729 25. Orvedahl A, Levine B. Viral evasion of autophagy. Autophagy. 2008;4: 280–5.
730 26. Sumpter R, Levine B. Selective autophagy and viruses. Autophagy. 2011;7: 260–5.
731 27. Ahmad L, Mostowy S, Sancho-Shimizu V. Autophagy-virus interplay: From cell biology
732 to human disease. Front Cell Dev Biol. 2018;6: 155.

733 28. Mohamud Y, Qu J, Xue YC, Liu H, Deng H, Luo H. CALCOCO2/NDP52 and
734 SQSTM1/p62 differentially regulate coxsackievirus B3 propagation. Cell Death Differ.
735 2019;26: 1062–76.
736 29. Cesarman E, Chang Y, Moore PS, Said JW, Knowles DM. Kaposi's sarcoma-associated
737 herpesvirus-like DNA sequences in AIDS-related body-cavity-based lymphomas. N Engl
738 J Med. 1995;332: 1186–91.
739 30. Chang Y, Cesarman E, Pessin MS, Lee F, Culpepper J, Knowles DM, et al. Identification
740 of herpesvirus-like DNA sequences in AIDS-associated Kaposi's sarcoma. Science.
741 1994;266: 1865–9.
742 31. Soulier J, Grollet L, Oksenhendler E, Cacoub P, Cazals-Hatem D, Babinet P, et al.
743 Kaposi's sarcoma-associated herpesvirus-like DNA sequences in multicentric Castleman's
744 disease. Blood. 1995;86: 1276–80.
745 32. Decker LL, Shankar P, Khan G, Freeman RB, Dezube BJ, Lieberman J, et al. The Kaposi
746 sarcoma-associated herpesvirus (KSHV) is present as an intact latent genome in KS tissue
747 but replicates in the peripheral blood mononuclear cells of KS patients. J Exp Med.
748 1996;184: 283–8.
749 33. Staskus KA, Zhong W, Gebhard K, Herndier B, Wang H, Renne R, et al. Kaposi's
750 sarcoma-associated herpesvirus gene expression in endothelial (spindle) tumor cells. J
751 Virol. 1997;71: 715–9.
752 34. Broussard G, Damania B. Regulation of KSHV Latency and Lytic Reactivation. Viruses.
753 MDPI AG; 2020;12: 1034.
754 35. Lee J-S, Li Q, Lee J-Y, Lee S-H, Jeong JH, Lee H-R, et al. FLIP-mediated autophagy
755 regulation in cell death control. Nat Cell Biol. 2009;11: 1355–62.

756 36. Leidal AM, Cyr DP, Hill RJ, Lee PWK, McCormick C. Subversion of autophagy by
757 Kaposi's sarcoma-associated herpesvirus impairs oncogene-induced senescence. Cell
758 Host Microbe. 2012;11: 167–80.
759 37. Young ARJ, Narita M, Ferreira M, Kirschner K, Sadaie M, Darot JFJ, et al. Autophagy
760 mediates the mitotic senescence transition. Genes Dev. 2009;23: 798–803.
761 38. Cougot N, Cavalier A, Thomas D, Gillet R. The Dual Organization of P-bodies Revealed
762 by Immunoelectron Microscopy and Electron Tomography. J Mol Biol. 2012;420: 17–28.
763 39. Hubstenberger A, Courel M, Bénard M, Souquere S, Ernoult-Lange M, Chouaib R, et al.
764 P-Body Purification Reveals the Condensation of Repressed mRNA Regulons. Mol Cell.
765 2017;68:144-157.
766 40. Corbet GA, Parker R. RNP granule formation: Lessons from P-bodies and stress granules.
767 Cold Spring Harb Symp Quant Biol. 2019;84: 203–15.
768 41. Youn JY, Dunham WH, Hong SJ, Knight JDR, Bashkurov M, Chen GI, et al. High-
769 Density Proximity Mapping Reveals the Subcellular Organization of mRNA-Associated
770 Granules and Bodies. Mol Cell. 2018;69: 517-532.
771 42. Riggs CL, Kedersha N, Ivanov P, Anderson P. Mammalian stress granules and P bodies at
772 a glance. J Cell Sci. 2020;133: jcs242487 .
773 43. Luo Y, Na Z, Slavoff SA. P-Bodies: Composition, Properties, and Functions.
774 Biochemistry. 2018;57: 2424.
775 44. Vindry C, Weil D, Standart N. Pat1 RNA-binding proteins: Multitasking shuttling
776 proteins. Wiley Interdiscip Rev RNA. 2019; 10: e1557
777 45.Barreau C, Paillard L, Osborne HB. AU-rich elements and associated factors: Are there
778 unifying principles? Nucleic Acids Res. Oxford University Press; 2005;33: 7138–50.

779 46. Bakheet T, Hitti E, Khabar KSA. ARED-Plus: An updated and expanded database of AU-
780 rich element-containing mRNAs and pre-mRNAs. Nucleic Acids Res. 2018;46:D218–20.
781 47. García-Mauriño SM, Rivero-Rodríguez F, Velázquez-Cruz A, Hernández-Vellisca M,
782 Díaz-Quintana A, De la Rosa MA, et al. RNA binding protein regulation and cross-talk in
783 the control of AU-rich mRNA Fate. Front Mol Biosci. 2017;4: 71.
784 48. Maitra S, Chou CF, Luber CA, Lee KY, Mann M, Chen CY. The AU-rich element mRNA
785 decay-promoting activity of BRF1 is regulated by mitogen-activated protein kinase-
786 activated protein kinase 2. RNA. 2008;14: 950–9.
787 49. Lai WS, Carballo E, Strum JR, Kennington EA, Phillips RS, Blackshear PJ. Evidence that
788 Tristetraprolin Binds to AU-Rich Elements and Promotes the Deadenylation and
789 Destabilization of Tumor Necrosis Factor Alpha mRNA. Mol Cell Biol. 1999;19: 4311–
790 23.
791 50. Lai WS, Blackshear PJ. Interactions of CCCH zinc finger proteins with mRNA.
792 Tristetraprolin-mediated AU-rich element-dependent mRNA degradation can occur in the
793 absence of a poly(A) tail. J Biol Chem. 2001;276: 23144–54.
794 51. Corcoran JA, Khaperskyy DA, Johnston BP, King CA, Cyr DP, Olsthoorn A V., et al.
795 Kaposi's Sarcoma-Associated Herpesvirus G-Protein-Coupled Receptor Prevents AU-
796 Rich-Element-Mediated mRNA Decay. J Virol. 2012;86:8859–71.
797 52. Corcoran JA, Johnston BP, McCormick C. Viral activation of MK2-hsp27-p115RhoGEF-
798 RhoA signaling axis causes cytoskeletal rearrangements, p-body disruption and ARE-
799 mRNA stabilization. PLoS Pathog. 2015;11:e1004597.
800 53. Franks TM, Lykke-Andersen J. TTP and BRF proteins nucleate processing body
801 formation to silence mRNAs with AU-rich elements. Genes Dev. 2007;21: 719–35.

802 54. Blanco FF, Sanduja S, Deane NG, Blackshear PJ, Dixon D a. Transforming growth factor
803 β regulates P-body formation through induction of the mRNA decay factor tristetraprolin.
804 Mol Cell Biol. 2014;34: 180–95.
805 55. Vindry C, Marnef A, Broomhead H, Twyffels L, Ozgur S, Stoecklin G, et al. Dual RNA
806 Processing Roles of Pat1b via Cytoplasmic Lsm1-7 and Nuclear Lsm2-8 Complexes. Cell
807 Rep. 2017;20:1187–200.
808 56. Ensoli B, Nakamura S, Salahuddin SZ, Biberfeld P, Larsson L, Beaver B, et al. AIDS-
809 Kaposi's Sarcoma-Derived Cells Express Cytokines with Autocrine and Paracrine Growth
810 Effects. Science. 2010;243:223–6.
811 57. Ensoli B, Stürzl M. Kaposi's sarcoma: a result of the interplay among inflammatory
812 cytokines, angiogenic factors and viral agents. Cytokine Growth Factor Rev. 1998;9: 63–
813 83.
814 58. Lane BR, Liu J, Bock PJ, Schols D, Coffey MJ, Strieter RM, et al. Interleukin-8 and
815 growth-regulated oncogene alpha mediate angiogenesis in Kaposi's sarcoma. J Virol.
816 2002;76: 11570–83.
817 59. Miles SA, Rezai AR, Salazar-González JF, Vander Meyden M, Stevens RH, Logan DM,
818 et al. AIDS Kaposi sarcoma-derived cells produce and respond to interleukin 6. Proc Natl
819 Acad Sci U S A. 1990;87: 4068–72.
820 60. Riva G, Barozzi P, Torelli G, Luppi M. Immunological and Inflammatory Features of
821 Kaposi's Sarcom and Other Kaposi's Sarcoma-Associated Herpesvirus/Human
822 Herpesvirus 8-Associated Neoplasias. AIDS Rev. 2010;9: 25–39.
823 61. Sadagopan S, Sharma-Walia N, Veettil MV, Raghu H, Sivakumar R, Bottero V, et al.
824 Kaposi's Sarcoma-Associated Herpesvirus Induces Sustained NF-κB Activation during

825 De Novo Infection of Primary Human Dermal Microvascular Endothelial Cells That Is
826 Essential for Viral Gene Expression. J Virol. 2007;8: 3949–68.
827 62. Salahuddin S, Nakamura S, Biberfeld P, Kaplan M, Markham P, Larsson L, et al.
828 Angiogenic properties of Kaposi's sarcoma-derived cells after long-term culture in vitro.
829 Science. 1988;242:430–3.
830 63. Corcoran JA, McCormick C. Viral activation of stress-regulated Rho-GTPase signaling
831 pathway disrupts sites of mRNA degradation to influence cellular gene expression. Small
832 GTPases. 2015;6: 178–85.
833 64. Standart N, Weil D. P-Bodies: Cytosolic Droplets for Coordinated mRNA Storage. Trends
834 Genet. 2018;34: 612–26.
835 65. Docena G, Rovedatti L, Kruidenier L, Fanning Á, Leakey NAB, Knowles CH, et al.
836 Down-regulation of p38 mitogen-activated protein kinase activation and proinflammatory
837 cytokine production by mitogen-activated protein kinase inhibitors in inflammatory bowel
838 disease. Clin Exp Immunol. 2010;162: 108–15.
839 66. Corcoran JA, Khaperskyy DA, McCormick C. Assays for monitoring viral manipulation
840 of host ARE-mRNA turnover. Methods. 2011;55: 172–81.
841 67. Wen KW, Damania B. Kaposi sarcoma-associated herpesvirus (KSHV): molecular
842 biology and oncogenesis. Cancer Lett. 2010;289: 140–50.
843 68. McCormick C, Ganem D. The Kaposin B Protein of KSHV Activates the p38/MK2
844 Pathway and Stabilizes Cytokine mRNAs. Science. 2005;307: 739–41.
845 69. Wei Y, An Z, Zou Z, Sumpter R, Su M, Zang X, et al. The stress-responsive kinases
846 MAPKAPK2/MAPKAPK3 activate starvation-induced autophagy through Beclin 1
847 phosphorylation. Elife. 2015;4: e05289.

848 70. Shen L, Qi Z, Zhu Y, Song X, Xuan C, Ben P, et al. Phosphorylated heat shock protein 27
849 promotes lipid clearance in hepatic cells through interacting with STAT3 and activating
850 autophagy. Cell Signal. 2016;28: 1086–98.
851 71. Gurkar AU, Chu K, Raj L, Bouley R, Lee S-H, Kim Y-B, et al. Identification of ROCK1
852 kinase as a critical regulator of Beclin1-mediated autophagy during metabolic stress. Nat
853 Commun. 2013;4: 2189.
854 72. Klionsky DJ, Abdel-Aziz AK, Abdelfatah S, Abdellatif M, Abdoli A, Abel S, et al.
855 Guidelines for the use and interpretation of assays for monitoring autophagy (4th edition).
856 Autophagy. 2021;17: 1-382.
857 73. Mizushima N, Murphy LO. Autophagy Assays for Biological Discovery and Therapeutic
858 Development. Trends Biochem Sci. 2020;45: 1080-1093.
859 74. Mizushima N, Yoshimori T, Levine B. Methods in Mammalian Autophagy Research.
860 Cell. 2010;140: 313–26.
861 75. Mauvezin C, Neufeld TP. Bafilomycin A1 disrupts autophagic flux by inhibiting both V-
862 ATPase-dependent acidification and Ca-P60A/SERCA-dependent autophagosome-
863 lysosome fusion. Autophagy. 2015;11:1437–8.
864 76. Kedersha N, Anderson P. Mammalian Stress Granules and Processing Bodies. Meth
865 Enzymol. 2007;431: 61-81.
866 77. Katayama H, Yamamoto A, Mizushima N, Yoshimori T, Miyawaki A. GFP-like proteins
867 stably accumulate in lysosomes. Cell Struct Funct. 2008;33: 1–12.
868 78. Thoreen CC, Kang SA, Won Chang J, Liu Q, Zhang J, Gao Y, et al. An ATP-competitive
869 Mammalian Target of Rapamycin Inhibitor Reveals Rapamycin-resistant Functions of
870 mTORC1. J Biol Chem. 2009;284: 8023–32.

871 79. Hardy SD, Shinde A, Wang W-H, Wendt MK, Geahlen RL. Regulation of epithelial-
872 mesenchymal transition and metastasis by TGF-β, P-bodies, and autophagy. Oncotarget.
873 2017;8: 103302–14.
874 80. Liu Q, Xu C, Kirubakaran S, Zhang X, Hur W, Liu Y, et al. Characterization of Torin2, an
875 ATP-competitive inhibitor of mTOR, ATM, and ATR. Cancer Res. 2013;73: 2574–86.
876 81. Kuang E, Tang Q, Maul GG, Zhu F. Activation of p90 Ribosomal S6 Kinase by ORF45 of
877 Kaposi's Sarcoma-Associated Herpesvirus and Its Role in Viral Lytic Replication. J Virol.
878 2008;82: 1838-50.
879 82. Kim J, Kundu M, Viollet B, Guan KL. AMPK and mTOR regulate autophagy through
880 direct phosphorylation of Ulk1. Nat Cell Biol. 2011;13: 132-41.
881 83. Alers S, Löffler AS, Wesselborg S, Stork B. Role of AMPK-mTOR-Ulk1/2 in the
882 Regulation of Autophagy: Cross Talk, Shortcuts, and Feedbacks. Mol Cell Biol. 2012;32:
883 2-11.
884 84. Kayyali US, Pennella CM, Trujillo C, Villa O, Gaestel M, Hassoun PM. Cytoskeletal
885 changes in hypoxic pulmonary endothelial cells are dependent on MAPK-activated protein
886 kinase MK2. J Biol Chem. 2002;277: 42596–602.
887 85. Rousseau S, Houle F, Landry J, Huot J. P38 MAP kinase activation by vascular
888 endothelial growth factor mediates actin reorganization and cell migration in human
889 endothelial cells. Oncogene. 1997;15: 2169–77.
890 86. Engel K, Schultz H, Martin F, Kotlyarov A, Plath K, Hahn M, et al. Constitutive
891 activation of mitogen-activated protein kinase-activated protein kinase 2 by mutation of
892 phosphorylation sites and an A-helix motif. J Biol Chem. 1995;270: 27213–21.
893 87. Guo L, Louis IV-S, Bohjanen PR. Post-transcriptional regulation of cytokine expression

894 and signaling. Curr Trends Immunol. 2018;19: 33–40.
895 88. Franks TM, Lykke-Andersen J. The control of mRNA decapping and P-body formation.
896 Mol Cell. 2008;32: 605–15.
897 89. Sharma-Walia N, Paul AG, Bottero V, Sadagopan S, Veettil MV, Kerur N, et al. Kaposi's
898 Sarcoma Associated Herpes Virus (KSHV) induced COX-2: A key factor in latency,
899 inflammation, angiogenesis, cell survival and invasion. PLoS Pathog. 2010;6: e1000777.
900 90. Ayache J, Bénard M, Ernoult-Lange M, Minshall N, Standart N, Kress M, et al. P-body
901 assembly requires DDX6 repression complexes rather than decay or Ataxin2/2L
902 complexes. Mol Biol Cell. 2015;26: 2579–95.
903 91. Guo H, Chitiprolu M, Gagnon D, Meng L, Perez-Iratxeta C, Lagace D, et al. Autophagy
904 supports genomic stability by degrading retrotransposon RNA. Nat Commun. 2014;5:
905 5276.
906 92. Myoung J, Ganem D. Generation of a doxycycline-inducible KSHV producer cell line of
907 endothelial origin: Maintenance of tight latency with efficient reactivation upon induction.
908 J Virol Methods. 2011;174: 12-21.
909 93. Kleer M, MacNeil G, Adam N, Pringle ES, Corcoran JA. A panel of KSHV mutants in the
910 polycistronic kaposin locus for precise analysis of individual protein products. J Virol.
911 2022;96: e0156021
912 94. Buchan JR, Kolaitis R, Taylor JP, Parker R. Eukaryotic Stress Granules Are Cleared by
913 Autophagy and Cdc48 / VCP Function. Cell. 2013;153: 1461–74.
914 95. Xie X, Li F, Wang Y, Wang Y, Lin Z, Cheng X, et al. Molecular basis of ubiquitin
915 recognition by the autophagy receptor CALCOCO2. Autophagy. 2015;11: 1775–89.
916 96. Cemma M, Kim PK, Brumell JH. The ubiquitin-binding adaptor proteins p62/SQSTM1

917 and NDP52 are recruited independently to bacteria-associated microdomains to target
918 Salmonella to the autophagy pathway. Autophagy. 2011;7: 341–5.
919 97. Yamano K, Youle RJ. Two different axes CALCOCO2-RB1CC1 and OPTN-ATG9A
920 initiate PRKN-mediated mitophagy. Autophagy. 2020;16: 2105–7.
921 98. Shi X, Chang C, Yokom AL, Jensen LE, Hurley JH. The autophagy adaptor ndp52 and the
922 fip200 coiled-coil allosterically activate ulk1 complex membrane recruitment. Elife.
923 2020;9: 1–20.
924 99. Dougherty JD, White JP, Lloyd RE. Poliovirus-mediated disruption of cytoplasmic
925 processing bodies. J Virol. 2011;85: 64–75.
926 100. Friedman E, Karen K. Effects of Adenovirus Infection on the Localization of Cellular
927 Protein Pat1b. Georg J Sci. 2017;75: 15.
928 101. Bish R, Cuevas-Polo N, Cheng Z, Hambardzumyan D, Munschauer M, Landthaler M, et
929 al. Comprehensive Protein Interactome Analysis of a Key RNA Helicase: Detection of
930 Novel Stress Granule Proteins. Biomolecules. 2015;5: 1441–66.
931 102. Gustafson EA, Wessel GM. DEAD-box helicases: posttranslational regulation and
932 function. Biochem Biophys Res Commun. 2010;395: 1–6.
933 103. Rahman H, Qasim M, Oellerich M, Asif AR. Crosstalk between Edc4 and mammalian
934 target of rapamycin complex 1 (mTORC1) signaling in mRNA decapping. Int J Mol Sci.
935 2014;15: 23179–95.
936 102. Yoon J-H, Choi E-J, Parker R. Dcp2 phosphorylation by Ste20 modulates stress granule
937 assembly and mRNA decay in Saccharomyces cerevisiae. J Cell Biol. 2010;189: 813–27.
938 105. Tenekeci U, Poppe M, Beuerlein K, Busch J, Schmitz ML, Kracht Correspondence M.
939 K63-Ubiquitylation and TRAF6 Pathways Regulate Mammalian P-Body Formation and

940 mRNA Decapping. Mol Cell. 2016;62: 943–57.
941 106. Aizer A, Kafri P, Kalo A, Shav-Tal Y. The P Body Protein Dcp1a Is Hyper-
942 phosphorylated during Mitosis. Prigent C, editor. PLoS One. 2013;8: e49783.
943 107. Chiang PY, Shen YF, Su YL, Kao CH, Lin NY, Hsu PH, et al. Phosphorylation of mRNA
944 Decapping Protein Dcp1a by the ERK Signaling Pathway during Early Differentiation of
945 3T3-L1 Preadipocytes. PLoS One. 2013;8: e61697.
946 108. Palanisamy V, Park NJ, Wang J, Wong DT. AUF1 and HuR proteins stabilize interleukin-
947 8 mRNA in human saliva. J Dent Res. 2008;87: 772–6.
948 109. Palanisamy V, Jakymiw A, Van Tubergen EA, D'Silva NJ, Kirkwood KL. Control of
949 Cytokine mRNA Expression by RNA-binding Proteins and microRNAs. J Dent Res.
950 2012;91: 651–8.
951 110. Lystad AH, Carlsson SR, de la Ballina LR, Kauffman KJ, Nag S, Yoshimori T, et al.
952 Distinct functions of ATG16L1 isoforms in membrane binding and LC3B lipidation in
953 autophagy-related processes. Nat Cell Biol. 2019;21: 372–83.
954 111. Ji E, Kim C, Kang H, Ahn S, Jung M, Hong Y, et al. RNA Binding Protein HuR Promotes
955 Autophagosome Formation by Regulating Expression of Autophagy-Related Proteins 5,
956 12, and 16 in Human Hepatocellular Carcinoma Cells. Mol Cell Biol. 2019;39: e00508-
957 18.
958 112. Yoo J, Kang J, Lee HN, Aguilar B, Kafka D, Lee S, et al. Kaposin-B enhances the
959 PROX1 mRNA stability during lymphatic reprogramming of vascular endothelial cells by
960 Kaposi's sarcoma herpes virus. PLoS Pathog. 2010;6: e1001046.
961 113. Pringle ES, Robinson C-A, McCormick C. Kaposi's Sarcoma-Associated Herpesvirus
962 Lytic Replication Interferes with mTORC1 Regulation of Autophagy and Viral Protein

963 Synthesis. J Virol. 2019;93: e00854-19.
964 114. Jo C, Gundemir S, Pritchard S, Jin YN, Rahman I, Johnson GVW. Nrf2 reduces levels of
965 phosphorylated tau protein by inducing autophagy adaptor protein NDP52. Nat Commun.
966 2014;5: 3496.
967 115. Moi P, Chan K, Asunis I, Cao A, Kan YW. Isolation of NF-E2-related factor 2 (Nrf2), a
968 NF-E2-like basic leucine zipper transcriptional activator that binds to the tandem NF-
969 E2/AP1 repeat of the β-globin locus control region. Proc Natl Acad Sci U S A. 1994;91:
970 9926–30.
971 116. Nguyen T, Nioi P, Pickett CB. The Nrf2-antioxidant response element signaling pathway
972 and its activation by oxidative stress. J Biol Chem. 2009;284: 13291–5.
973 117. Gjyshi O, Bottero V, Veettil MV, Dutta S, Singh VV, Chikoti L, et al. Kaposi's sarcoma-
974 associated herpesvirus induces Nrf2 during de novo infection of endothelial cells to create
975 a microenvironment conducive to infection. PLoS Pathog. 2014;10: e1004460.
976 118. Gjyshi O, Flaherty S, Veettil MV, Johnson KE, Chandran B, Bottero V. Kaposi's
977 Sarcoma-Associated Herpesvirus Induces Nrf2 Activation in Latently Infected Endothelial
978 Cells through SQSTM1 Phosphorylation and Interaction with Polyubiquitinated Keap1. J
979 Virol. 2015;89: 2268–86.
980 119. Vescovo T, Pagni B, Piacentini M, Fimia GM, Antonioli M. Regulation of Autophagy in
981 Cells Infected With Oncogenic Human Viruses and Its Impact on Cancer Development.
982 Front Cell Dev Biol. 2020;8: 47.
983 120. Liu J, Debnath J. The Evolving, Multifaceted Roles of Autophagy in Cancer. Adv Cancer
984 Res. 2016;130: 1–53.
985 121. Wu WKK, Coffelt SB, Cho CH, Wang XJ, Lee CW, Chan FKL, et al. The autophagic

986 paradox in cancer therapy. Oncogene. 2012;31: 939–53.
987 122. Kuma A, Hatano M, Matsui M, Yamamoto A, Nakaya H, Yoshimori T, et al. The role of
988 autophagy during the early neonatal starvation period. Nature. 2004;432: 1032–6.
989 123. Yoo SM, Ahn AK, Seo T, Hong HB, Chung MA, Jung SD, et al. Centrifugal enhancement
990 of Kaposi's sarcoma-associated virus infection of human endothelial cells in vitro. J Virol
991 Methods. 2008;154: 160-6.
992 124. Castle EL, Robinson C-A, Douglas P, Rinker KD, Corcoran JA. Viral manipulation of a
993 mechanoresponsive signaling axis disassembles processing bodies. Mol Cell Biol.
994 2021;41: e0039921.
995 125. Horn M, Geisen C, Cermak L, Becker B, Nakamura S, Klein C, et al. DRE-1/FBXO11-
996 dependent degradation of BLMP-1/BLIMP-1 governs C. elegans developmental timing
997 and maturation. Dev Cell. 2014;28: 697-710.
998 126. Moffat J, Grueneberg DA, Yang X, Kim SY, Kloepfer AM, Hinkle G, et al. A Lentiviral
999 RNAi Library for Human and Mouse Genes Applied to an Arrayed Viral High-Content
1000 Screen. Cell. 2006;124: 1283–98.
1001 127. Bryant DM, Datta A, Rodríguez-Fraticelli AE, PeräCurrency Signnen J, Martín-Belmonte
1002 F, Mostov KE. A molecular network for de novo generation of the apical surface and
1003 lumen. Nat Cell Biol. 2010;12: 1035–45.
1004 128. Johnston BP, Pringle ES, McCormick C. KSHV activates unfolded protein response
1005 sensors but suppresses downstream transcriptional responses to support lytic replication.
1006 PLoS Pathog. 2019;15: e1008185.
1007 129. Sancak Y, Peterson TR, Shaul YD, Lindquist RA, Thoreen CC, Bar-Peled L, et al. The rag
1008 GTPases bind raptor and mediate amino acid signaling to mTORC1. Science. 2008;320:

1009 1496-501.

1010 130. Tritschler F, Braun JE, Motz C, Igreja C, Haas G, Truffault V, et al. DCP1 forms

1011 asymmetric trimers to assemble into active mRNA decapping complexes in metazoa. Proc

1012 Natl Acad Sci U S A. 2009;106: 21591-6.

1013 131. Marnef A, Weil D, Standart N. RNA-related nuclear functions of human Pat1b, the P-

1014 body mRNA decay factor. Mol Biol Cell. 2012;23: 213-24.

1015

1016
1017

1018 **Figure Legends**

1019 **Figure 1: Kaposin B increases autophagic flux.** Primary human umbilical vein endothelial
1020 cells (HUVECs) were transduced with recombinant lentiviruses expressing either Kaposin B
1021 (KapB) or an empty vector control and selected with blasticidin (5 µg/mL). A: Cells were treated
1022 with Bafilomycin A1 (BafA1, 10 nM) or a vehicle control (DMSO) for the indicated times prior
1023 to harvest in 2x Laemmli buffer. Protein lysates were resolved by SDS-PAGE and immunoblot
1024 was performed for p62 and LC3. Samples were quantified using Image Lab (Biorad) software
1025 and then normalized, first to total protein and then to their respective starting time points (0 h).
1026 Results were plotted in GraphPad and a linear regression statistical test was performed, ±SEM;
1027 n=3, *=P<0.05, ***=P<0.001. B: Cells were treated with BafA1 for 30 min prior to fixation in
1028 methanol. Immunofluorescence was performed for LC3 (white) and DAPI (nuclei, blue). Scale
1029 bar=20 µm. Total LC3 area per field was quantified by identifying LC3-positive puncta using
1030 CellProfiler and normalizing to the number of nuclei and the vector DMSO control. Results were
1031 plotted in GraphPad, a 2-way ANOVA was performed with a Šidák's multiple comparison test,
1032 matched data from each replicate was paired for comparison, ±SEM; n=3, *=P<0.05. C:
1033 HUVECs were transduced with recombinant lentiviruses expressing either Kaposin B (KapB) or
1034 an empty vector control and selected with blasticidin (5 µg/mL). Cells were treated with sodium
1035 arsenite (0.25 mM) or a vehicle control for 30 min prior to fixation in 4% paraformaldehyde and
1036 permeabilization in 0.1% Triton X-100. Scale bar=20 µm. Hedls puncta were quantified using
1037 CellProfiler and presented as number of Hedls puncta per cell, all cells counted are displayed.
1038 Results were plotted in GraphPad and a 2-way ANOVA was performed on the main column
1039 effects with a Tukey's multiple comparison test, bar represents the mean; n=3, **=P<0.01,
1040 ****=P<0.0001.

1041 **Figure 2: Kaposin B requires canonical autophagy to disassemble PBs.** A & B: HUVECs
1042 were sequentially transduced: first with recombinant lentiviruses expressing either shRNAs
1043 targeting Atg5 (C) or Atg14 (D) (shAtg5, shAtg14) or a non-targeting control (NS) and selected
1044 with puromycin (1 µg/mL), and second with either KapB or an empty vector control and selected
1045 with blasticidin (5 µg/mL). Coverslips were fixed in 4% paraformaldehyde, permeabilized in
1046 0.1% Triton X-100, and immunostained for the PB-resident protein Hedls (white) and nuclei
1047 (DAPI). Scale bar=20 µm. Hedls puncta were quantified using CellProfiler and presented as
1048 number of Hedls puncta per cell, all cells counted are displayed. Results were plotted in
1049 GraphPad and a 2-way ANOVA was performed on the main column effects with a Tukey's
1050 multiple comparison test, bar represents the mean; n=4 (C), n=3 (D), ****=P<0.0001. C:
1051 HUVECs were treated as in B. Coverslips were fixed in 4% paraformaldehyde, permeabilized in
1052 0.1% Triton X-100, and immunostained for the PB-resident protein Hedls (white) and nuclei
1053 (DAPI). Scale bar=20 µm. Hedls puncta were quantified using CellProfiler and presented as
1054 number of Hedls puncta per cell, all cells counted are displayed. Results were plotted in
1055 GraphPad and a 2-way ANOVA was performed on the main column effects with a Tukey's
1056 multiple comparison test, bar represents the mean; n=3, **=P<0.01.
1057
1058 **Figure 3: Torin treatment disassembles PBs.** A: HUVECs were treated with either Torin (250
1059 nM) or a DMSO control for 2 h prior to fixation in 4% paraformaldehyde. Samples were
1060 permeabilized in 0.1% Triton X-100. Immunofluorescence was performed for Hedls (PBs, white)
1061 and DAPI (nuclei, blue). Scale bar=20 µm. Hedls puncta were quantified using CellProfiler and
1062 presented as number of Hedls puncta per cell, all cells counted are displayed. Results were
1063 plotted in GraphPad and a 2-way ANOVA was performed on the main column effects with a

1064 Tukey's multiple comparison test, bar represents the mean; n=3, ****=P<0.0001. B: HUVECs
1065 were treated with either Torin (250 nM) or a DMSO control for 90 min prior to the addition of
1066 sodium arsenite (0.25 mM) for 30 min. Cells were fixed in 4% paraformaldehyde and
1067 permeabilized in 0.1% Triton X-100. Immunofluorescence was performed for Hedls (PBs, white)
1068 and DAPI (nuclei, blue). Scale bar=20 µm. Hedls puncta were quantified using CellProfiler and
1069 presented as number of Hedls puncta per cell, all cells counted are displayed. Results were
1070 plotted in GraphPad and a 2-way ANOVA was performed on the main column effects with a
1071 Tukey's multiple comparison test, bar represents the mean; n=3, *=P<0.05. C: HUVECs were
1072 transduced with recombinant lentiviruses expressing either KapB, constitutively active MK2
1073 (MK2EE), or an empty vector control and selected with blasticidin (5 µg/mL). Cells were treated
1074 with either Torin (250 nM) or a DMSO control for 2 h prior to harvest in 2x Laemmli buffer.
1075 Protein lysates were resolved by SDS-PAGE and immunoblot was performed for phospho-S6
1076 (Ser235/236) and total S6. D: HUVECs were transduced and treated as in C and harvested in 2X
1077 Laemmli buffer. Protein lysates were resolved by SDS-PAGE and immunoblot was performed
1078 for phospho-ULK (Ser757), phospho-ULK (Ser555), and total ULK. E: HUVECs were
1079 transduced as in C and harvested in 2X Laemmli buffer. Protein lysates were resolved by SDS-
1080 PAGE and immunoblot was performed for phospho-Beclin 1 (Ser90) and total Beclin 1. Samples
1081 were quantified by normalizing total and phospho-Beclin 1 protein levels to the total protein in
1082 each lane and then using Image Lab (Biorad), normalizing to the Vector control, and then
1083 dividing phospho- over total Beclin 1. Results were plotted in GraphPad and a one-way
1084 ANOVA was performed with a Dunnett's test, ±SEM; n=4, *=P<0.05.
1085

1086 **Figure 4: KapB-mediated ARE-mRNA reporter expression requires canonical autophagy.**
1087 A: HUVECs were transduced with recombinant lentiviruses expressing either KapB or an empty
1088 vector control and selected with blasticidin (5 µg/mL). Conditioned media harvested from
1089 r.219.KSHV latently infected iSLK cells was used to mimic the KS lesion microenvironment and
1090 induce the transcription of cytokines for 6 h prior to lysis for total RNA, normal media was used
1091 for the 0 h time point. Transcript levels were quantified by qPCR and normalized to 18S as a
1092 reference gene. Data is represented as the fold change in target transcript expression relative to
1093 the untreated vector control and was quantified using the ΔΔCq method. Results were plotted in
1094 GraphPad, a 2-way ANOVA was performed, ±SEM; n=3, *=P<0.05, **=P<0.01. B: HUVECs
1095 were treated with Torin (250 nM) or a DMSO control for 2 h prior to lysis for total RNA.
1096 Transcript levels were quantified by qPCR and normalized to HPRT as a reference gene. Data is
1097 represented as the fold change in target transcript expression relative to the untreated vector
1098 control and was quantified using the ΔΔCq method. An unpaired t-test was performed, ±SEM;
1099 n=3, *=P<0.05. C: HeLa Tet-Off cells were co-transfected with expression plasmids for an ARE-
1100 containing firefly luciferase plasmid (pTRE-FLuc-ARE) and a stable renilla luciferase plasmid
1101 (pTRE-RLuc). 36 h post transfection, doxycycline (Dox) was added to halt reporter gene
1102 transcription of both luciferase reporters, at the same time Torin (250 nM) or DMSO were added;
1103 12 h after Dox addition, lysates were harvested in passive lysis buffer (Promega). Luciferase
1104 activity for both FLuc and RLuc was analyzed using the Dual-Luciferase Reporter Assay
1105 (Promega) and normalized (FLuc/RLuc) relative luciferase was calculated in relative light units
1106 (RLUs). Results were plotted using GraphPad, an unpaired t-test was performed, ±SEM; n=6,
1107 ***=P<0.001. D&E: HeLa Tet-Off cells were transduced with recombinant lentiviruses
1108 expressing either shRNAs targeting Atg5 or Atg14 (shAtg5, shAtg14) or a non-targeting control

1109 (NS) and selected with puromycin (1 µg/mL). After selection, cells were co-transfected and Dox
1110 treatment was performed as described in C, except that co-transfection also included an
1111 expression plasmid for KapB or an empty vector control. Results were plotted using GraphPad,
1112 an unpaired t-test was performed, ±SEM; n=3, *=P<0.05, **=P<0.01. F: Cells were co-
1113 transfected as in E and BafA1 (10 nM) was added at the same time as Dox. Results were plotted
1114 in GraphPad and a Student's t-test was performed, ±SEM; n=3, *=P<0.05, **=P<0.01.
1115
1116 **Figure 5: Dcp1a protein levels are decreased by KapB expression and Torin treatment.** A:
1117 HUVECs were treated with DMSO or Torin (250 nM) for 4 h prior to harvest. Samples were
1118 lysed in 2x Laemmli buffer and resolved by SDS-PAGE before immunoblotting with Xrn1,
1119 EDC4/Hedls, Dcp1a, and DDX6. Samples were quantified by normalizing the PB resident
1120 protein levels to the total protein in each lane and then the DMSO control using ImageLab
1121 (Biorad). Results were plotted in GraphPad and a one-way ANOVA was performed ±SEM; n=3,
1122 **=P<0.01. B: HUVECs were transduced with recombinant lentiviruses expressing either KapB
1123 or an empty vector control and selected with blasticidin (5 µg/mL). Cells were treated with
1124 DMSO or bafilomycin A1 (BafA1, 10 nM) for 4 h prior to harvest in 2x Laemmli buffer.
1125 Samples were resolved by SDS-PAGE and immunoblot was performed for Dcp1a or p62
1126 (autophagy marker). Samples were quantified by normalizing Dcp1a protein levels to the total
1127 protein in each lane using Image Lab (Biorad) and then to the Vector DMSO control.
1128 Representative blot is from the same membrane, hashed line indicates skipped lanes. Results
1129 were plotted in GraphPad and a 2-way ANOVA was performed, ±SEM; n=3, ***=P<0.001. C:
1130 HUVECs were transduced with recombinant lentiviruses expressing either KapB or an empty
1131 vector control and selected with blasticidin (5 µg/mL). Samples were harvested in 2x Laemmli

1132 buffer, resolved by SDS-PAGE and immunoblot was performed for Xrn1, Hedls/EDC4, or
1133 DDX6. Samples were quantified by normalizing PB protein levels to the total protein in each
1134 lane using Image Lab (Biorad) and then to the Vector control. Results were plotted in GraphPad.
1135 D: HUVECs were sequentially transduced: first with recombinant lentiviruses expressing either
1136 shRNAs targeting Atg5 (shAtg5) or a non-targeting control (NS) and selected with puromycin (1
1137 µg/mL), and second with either KapB or an empty vector control and selected with blasticidin (5
1138 µg/mL). Samples were harvested in 2x Laemmli buffer and resolved by SDS-PAGE.
1139 Immunoblot was performed for Dcp1a, Atg5, and KapB. Samples were quantified by
1140 normalizing Dcp1a protein levels to the total protein in each lane using Image Lab (Biorad) and
1141 then to the Vector NS control. Results were plotted in GraphPad and a 2-way ANOVA was
1142 performed, ±SEM; n=3, *=P<0.05, **P=<0.01.
1143
1144 **Figure 6: KapB-mediated PB disassembly and ARE-mRNA reporter expression require the**
1145 **selective autophagy receptor NDP52**. A: HUVECs were sequentially transduced with
1146 recombinant lentivirus expressing KapB or an empty vector control and selected with blasticidin
1147 (5 µg/mL), and second with shRNAs targeting NDP52 or a non-targeting control (NS) and
1148 selected with puromycin (1 µg/mL). Coverslips were fixed in 4% paraformaldehyde,
1149 permeabilized in 0.1% Triton X-100 and immunostained for Hedls (PBs; white), DAPI (nuclei,
1150 blue). Scale bar=20 µm. Hedls puncta were quantified using CellProfiler and presented as
1151 number of Hedls puncta per cell, all cells counted are displayed. Results were plotted in
1152 GraphPad and a 2-way ANOVA was performed on the main column effects with a Tukey's
1153 multiple comparison test, bar represents the mean; n=3, *=P<0.05. B: HUVECs were transduced
1154 with recombinant lentivirus expressing an shRNA targeting NDP52 and selected with puromycin

1155 (1 µg/mL). Cells were treated with Torin (250 nM) or a DMSO control for 2 h prior to fixation in
1156 4% paraformaldehyde and permeabilization in 0.1% Triton X-100. Samples were immunostained
1157 for Hedls (PBs; white), DAPI (nuclei, blue). Scale bar=20 µm. Hedls puncta were quantified
1158 using CellProfiler and presented as number of Hedls puncta per cell, all cells counted are
1159 displayed. Results were plotted in GraphPad and a 2-way ANOVA was performed on the main
1160 column effects with a Tukey's multiple comparison test, bar represents the mean; n=3,
1161 ****=P<0.0001. C: HUVECs were transduced with recombinant lentiviruses expressing either
1162 an shRNA targeting NDP52 or a non-targeting control (NS) and selected with puromycin (1
1163 µg/mL). Cells were treated with DMSO or Torin (250 nM) for 4 h prior to harvest in 2x Laemmli
1164 buffer. Samples were resolved by SDS-PAGE and immunoblot was performed for Dcp1a, Pat1b
1165 or DDX6. Samples were quantified by normalizing Dcp1a or Pat1b protein levels to the total
1166 protein in each lane using Image Lab (Biorad) and then to the NS DMSO control. Results were
1167 plotted in GraphPad and a 2-way ANOVA was performed, ±SEM; n=3 (Dcp1a) n=4 (Pat1b),
1168 *=P<0.05. D: HeLa Tet-Off cells were transduced with recombinant lentivirus expressing
1169 shRNAs targeting NDP52, OPTN, p62 or a NS control and selected with puromycin (1µg/mL)
1170 then cells were co-transfected, treated with Dox and luciferase activity was recorded and
1171 analyzed as in Figure 3. Data were plotted in GraphPad as the mean fold change in the relative
1172 luciferase activity of each condition compared to vector NS or KapB NS; n=4. An unpaired t-test
1173 was performed; * = P<0.05 **= P<0.01. E: HUVECs were sequentially transduced first with
1174 recombinant lentivirus expressing shDNP52 targeting the 3'-UTR of NDP52 or a NS control and
1175 selected with blasticidin (5 µg/mL), and second, with KapB and either mCherry control (mCh) or
1176 RFP-NDP52. Coverslips were fixed with 4% paraformaldehyde, permeabilized with 0.1% Triton
1177 X-100, and immunostained with Hedls (PBs, green). Scale bar=20 µm. F: Samples from E were

1178 quantified; Hedls puncta were quantified using CellProfiler and presented as number of Hedls
1179 puncta per cell, all cells counted are displayed. Results were plotted in GraphPad and a 2-way
1180 ANOVA was performed on the main column effects with a Tukey's multiple comparison test,
1181 bar represents the mean; n=3, ****=P<0.0001.
1182
1183 **Figure 7: KSHV infection induces autophagic flux and phosphorylation of Beclin 1.** A:
1184 HUVECs were infected with rKSHV.219 via spinoculation and infection was allowed to proceed
1185 for 96 h prior to treatment with bafilomycin A1 (10 nM) for 30 min. Coverslips were fixed in
1186 methanol and immunostained for LC3 (autophagosomes; white) and DAPI (nuclei, blue). Cells
1187 were visually assessed for infection via viral latency associated nuclear antigen (LANA)
1188 immunofluorescence. Scale bar=20 µm. Total LC3 area per field was quantified by identifying
1189 LC3 puncta using CellProfiler and normalizing to the number of nuclei and the Mock DMSO
1190 control. Results were plotted in GraphPad and a 2-way ANOVA was performed with a Šidák's
1191 multiple comparison test, ±SEM n=5; *=P<0.05. B: Naïve iSLK cells were infected with wild-
1192 type (WT) or delete KapB (delB) BAC16 KSHV via spinoculation, robust and stable latency was
1193 achieved by expanding and selecting cells in hygromycin B (500 µg/mL and then 1200 µg/mL)
1194 for one week before seeding for experiments. Cells were treated with Bafilomycin A1 (BafA1,
1195 10 nM) or a vehicle control (DMSO) for the indicated times prior to harvest in 2x Laemmli
1196 buffer. Protein lysates were resolved by SDS-PAGE and immunoblot was performed for p62 and
1197 LC3. Samples were quantified using Image Lab (Biorad) software and then normalized, first to
1198 total protein and then to their respective starting time points (0 h). Results were plotted in
1199 GraphPad and a linear regression statistical test was performed, ±SEM; n=3, *=P<0.05. C:
1200 HUVECs were infected as in A for 96 h and harvested in 2x Laemmli buffer. Protein lysates

1201 were resolved by SDS-PAGE and immunoblot was performed for phosphor-Beclin 1 (S90) and
1202 total Beclin 1. Samples were quantified using Image Lab (Biorad) software and then normalized,
1203 first to total protein and then to the Mock control. Results were plotted in GraphPad and a
1204 Student's t-test was performed, ±SEM n=3; *=P<0.05. D: HUVECs were infected with wild-
1205 type (WT) or delete KapB (delB) BAC16 KSHV via spinoculation and infection was allowed to
1206 proceed for 96 h prior to treatment with bafilomycin A1 (10 nM) for 30 min. Coverslips were
1207 fixed in methanol and immunostained for LC3 (autophagosomes; white) and DAPI (nuclei,
1208 blue). Cells were visually assessed for infection via viral LANA immunofluorescence. Scale
1209 bar=20 µm. Total LC3 area per field was quantified by identifying LC3 puncta using CellProfiler
1210 and normalizing to the number of nuclei and the Mock DMSO control. Results were plotted in
1211 GraphPad and a 2-way ANOVA was performed with a Šidák's multiple comparison test, ±SEM
1212 n=3; *P<0.05. E: HUVECs were infected as in C for 96 h and harvested in 2x Laemmli buffer.
1213 Protein lysates were resolved by SDS-PAGE and immunoblot was performed for phospho-
1214 Beclin 1 (S90) and total Beclin 1. Samples were quantified using Image Lab (Biorad) software
1215 and then normalized, first to total protein and then to the Mock control. Results were plotted in
1216 GraphPad and a one-way ANOVA was performed, ±SEM n=3; *=P<0.05.

1217

1218 **Figure 8: KSHV-mediated PB disassembly requires Atg5 and the selective autophagy**
1219 **receptor NDP52.** A: HUVECs were transduced with recombinant lentivirus expressing shRNAs
1220 targeting Atg5, NDP52, or a non-targeting control (NS) and selected with puromycin (1 µg/mL).
1221 Cells were infected with rKSHV.219 via spinoculation and infection was allowed to proceed for
1222 96 h. Coverslips were fixed in 4% paraformaldehyde, permeabilized in 0.1% Triton X-100 and
1223 immunostained for Hedls (PBs; white), LANA (KSHV latency, green), and DAPI (nuclei, blue).

1224 Scale bar=20 µm. Hedls puncta were quantified using CellProfiler and presented as number of
1225 Hedls puncta per cell, all cells counted are displayed. Results were plotted in GraphPad and a 2-
1226 way ANOVA was performed on the main column effects with a Tukey's multiple comparison
1227 test, bar represents the mean; n=3, *=P<0.05. B: HUVECs were transduced with recombinant
1228 lentiviruses and infected with rKSHV.219 as in A. Cells were harvested in 2X Laemmli buffer.
1229 Protein lysates were resolved by SDS-PAGE and immunoblot was performed for Atg5 and
1230 NDP52. C: HUVECs were infected with rKSHV.219 via spinoculation and infection was
1231 allowed to proceed for 96 h. Cells were harvested in 2x Laemmli buffer. Samples were resolved
1232 by SDS-PAGE and immunoblot was performed for NDP52. Samples were quantified by
1233 normalizing NDP52 protein levels to the total protein in each lane using Image Lab (Biorad) and
1234 then to Mock. Results were plotted in GraphPad and an unpaired t-test was performed, ±SEM;
1235 n=3, *=P<0.05. D: HEK293T cells were transfected with plasmids expressing pcDNA-FLAG-
1236 NDP52 with either pLJM1-GFP (control), pLJM1-GFP-Dcp1a, or pLJM1-GFP-Pat1b for 48 h.
1237 Cells were harvested in lysis buffer and incubated with a FLAG mouse antibody (CST) overnight
1238 at 4 °C. Immunoprecipitation was performed and samples were eluted from the magnetic beads
1239 through boiling in 4x Laemmli buffer (Biorad) with 10% v/v beta-mercaptoethanol. Samples
1240 were resolved by SDS-PAGE. A representative blot of three independent experiments is shown.
1241 E: HUVECs were infected with rKSHV.219 via spinoculation and infection was allowed to
1242 proceed for 96 h. Cells were harvested in 2x Laemmli buffer. Samples were resolved by SDS-
1243 PAGE and immunoblot was performed for Dcp1a or Pat1b. Samples were quantified by
1244 normalizing Dcp1a or Pat1b protein levels to the total protein in each lane using Image Lab
1245 (Biorad) and then to Mock. Results were plotted in GraphPad and an unpaired t-test was
1246 performed, ±SEM; n=3, **=P<0.01. F:. Model of PB disassembly induced by KSHV/KapB.

1247 KapB increases the phosphorylation of Beclin 1 at Serine 90 to enhance autophagic flux while
1248 Torin induces autophagic flux via the inhibition of mTORC1/2 and dephosphorylation of the
1249 ULK complex. Enhanced activation of autophagic flux by either mechanism results in PB
1250 disassembly that is dependent on the selective autophagy receptor, NDP52. In our model, we
1251 predict that NDP52 recruits a PB component(s) to the nascent autophagosome. Our top candidate
1252 for this recruitment is the PB scaffolding protein, Pat1b, as NDP52 co-immunoprecipitated with
1253 Pat1b consistent with Pat1b protein level decreases after KSHV infection and Torin treatment.
1254 Steady state levels of Dcp1a also decreased in response to KapB expression, KSHV infection or
1255 Torin treatment, suggesting that Dcp1a decreases may be mediated by its interaction with Pat1b.
1256 Autophagic degradation of Pat1b and Dcp1a lead to PB disassembly.
1257
1258
1259

1260 **Tables**

1261 Table 1: Drugs

Drug	Vendor/Catalogue #	Concentration
Torin1	Sigma-Aldrich 475991	250 nM
Bafilomycin A1	Sigma-Aldrich B1793	10 nM
Chloroquine	Sigma-Aldrich C6628	25 µM
MG-132	Selleckchem S2619	5 µM
LPS	Sigma-Aldrich L3129	1 µg/mL
Sodium Arsenite	Sigma-Aldrich 1.06277	0.25 mM
Doxycycline	Sigma-Aldrich D9891	1 µg/mL
Hygromycin B	ThermoFisher 10687010	500 or 1200 µg/mL

1262

1263 Table 2: Plasmids

Plasmid	Use	Source	Mammalian Selection
RFP-NDP52	Cloning	Dr. Andreas Till (University Hospital of Bonn)	N/A
pcDNA 3.1 (+)	Empty Vector Control	Invitrogen V79020	N/A
FLAG-HA-pcDNA	Empty Vector Control Co-IP	Addgene #52535 (125)	N/A
pcDNA KapB BCBL1	ARE-mRNA stability	(52)	N/A
pcDNA FLAG-MK2EE	ARE-mRNA stability	(52)	N/A
pLKO.1-TRC	shRNA expression	Addgene #10878 (126)	Puromycin
pLKO.1-blast	shRNA expression	Addgene #26655(127)	Blasticidin
pLJM1	Empty Vector Control	(128)	Blasticidin/ Puromycin
pLJM1 KapB (pulmonary KS)	Overexpression	Cloned from pBMNIP-KapB (52) into pLJM1-BSD	Blasticidin
pLJM1 mCh	Overexpression Control	Craig McCormick (Dalhousie University)	Blasticidin
pLJM1 FLAG-MK2EE	Overexpression	Cloned into pLJM1 using BamHI and EcoRI from pBMN FLAG-MK2EE (52)	Blasticidin/ Puromycin
pLJM1 RFP-NDP52	Overexpression	Cloned into pLJM1 using NheI and BamHI from RFP-NDP52	Puromycin
pcDNA-FLAG-NDP52	Co-IP	Cloned using primers listed in Table 4 from RFP-NDP52	N/A
pLJM1-EGFP	Co-IP	Addgene #19319 (129)	Puromycin
pT7-EGFP-C1-HsDcp1a	Cloning	Addgene #25030 (130)	N/A
pLJM1-GFP-Dcp1a	Co-IP	Cloned into pLJM1 using AgeI and EcoRI from pT7-EGFP-C1-HsDcp1a	Puromycin

Plasmid	Use	Source	Mammalian Selection
Pat1b-GFP	Cloning	(131)	N/A
pLJM1-GFP-Pat1b	Co-IP	Cloned into pLJM1 using NheI and BamHI from GFP-Pat1b	Puromycin
pMD2.G	Lentivirus generation	Addgene #12259	N/A
psPAX2	Lentivirus generation	Addgene #12260	N/A
pTRE2 Firefly Luciferase-ARE	ARE-mRNA stability	(66)	N/A
pTRE2-Renilla Luciferase	ARE-mRNA stability	(66)	N/A

1264

1265 Table 3: shRNA target sequences

shRNA target	shRNA sequence 5'→3'	Region
Non-targeting (NS)	AGCACAAGCTGGAGTACAACTA	
Atg14	GTCTGGCAAATCTTCGACGAT	CDS
Atg5	CTTTGATAATGAACAGTGAGA	CDS
NDP52(1)	GAGCTGCTTCAACTGAAAGAA	CDS
NDP52(2)	GACTTGCCTATGGAAACCCAT	CDS
NDP52(3)	CCCTTTGTGAACTAAGTTCAA	3'-UTR
NDP52(4)	CCTGACTTGATACTAAGTGAT	3'-UTR
Optineurin (1)	GCACGGCATTGTCTAAATATA	CDS
Optineurin (2)	GCCATGAAGCTAAATAATCAA	CDS
p62	CCGAATCTACATTAAAGAGAA	CDS
NBR1 (1)	GCCAGGAACCAAGTTTATCAA	CDS
NBR1 (2)	CCATCCTACAATATCTGTGAA	CDS
VCP (1)	ACCGTCCCAATCGGTTAATTG	CDS
VCP (2)	AGATCCGTCGAGATCACTTTG	CDS

1266

1267 Table 4: Cloning Primers

Primer	Primer sequence
NDP52-EcoRI-Forward	5' ACCGGTCCATGGAGGAGACCATCAAA 3'
NDP52-BamHI-Reverse	5' CCGGTGGATCCTCAGAGAGA 3'

1268

1269

1270 Table 5: Antibodies

Antibody	Species	Vendor/Catalogue #	Application	Dilution
Hedls	Mouse	Santa Cruz sc-8418	Immunofluorescence Immunoblot	1:1000 1:1000
KapB	Rabbit	A generous gift from Don Ganem	Immunofluorescence	1:1000
NDP52	Rabbit	CST 60732	Immunoblot	1:1000
p62	Rabbit	CST 7695	Immunoblot	1:1000
Dcp1a	Mouse	CST 15365	Immunoblot	1:500
DDX6	Rabbit	Bethyl A300-461	Immunoblot	1:1000

Pat1b	Rabbit	CST 14288	Immunoblot	1:500
LC3B	Rabbit	CST 2775	Immunofluorescence Immunoblot	1:200 1:1000
Atg5	Rabbit	CST 2630	Immunoblot	1:1000
Atg14	Rabbit	CST 96752	Immunoblot	1:1000
OPTN	Rabbit	Abcam ab23666	Immunoblot	1:1000
Xrn1	Rabbit	Abcam ab231197	Immunoblot	1:1000
VCP	Rabbit	CST 2649	Immunoblot	1:1000
NBR1	Rabbit	CST 9891	Immunoblot	1:1000
LANA	Rabbit	A generous gift from Don Ganem	Immunofluorescence	1:1000
Phospho-S6 (Ser235/236)	Rabbit	CST 4858	Immunoblot	1:1000
Total S6	Rabbit	CST 2217	Immunoblot	1:1000
Phospho-Beclin 1 (Ser90)	Rabbit	CST 86455	Immunoblot	1:500
Total Beclin 1	Mouse	CST 4122	Immunoblot	1:1000
Phospho-ULK (Ser555)	Rabbit	CST 5869	Immunoblot	1:1000
Phospho-ULK (Ser757)	Rabbit	CST 14202	Immunoblot	1:1000
Total ULK	Rabbit	CST 8054	Immunoblot	1:1000
FLAG	Rabbit	CST 14793	Immunoblot	1:1000
FLAG	Mouse	CST 8146	Immunoprecipitation	1:100
GFP	Rabbit	CST 2956	Immunoblot	1:1000

Table 6: qPCR primers

Primer	**Primer Sequence**
HPRT-1- Forward	5’ CTTTCCTTGGTCAGGCAGTATAA 3’
HPRT-1 - Reverse	5’ AGTCTGGCTTATATCCAACACTTC 3’
18S - Forward	5’ TTCGAACGTCTGCCCTATCAA 3’
18S - Reverse	5’ GATGTGGTAGCCGTTTCTCAGG 3’
IL-6 - Forward	5’ GAAGCTCTATCTCGCCTCCA 3’
IL-6 - Reverse	5’ TTTTCTGCCAGTGCCTCTTT 3’
CXCL8 - Forward	5’ AAATCTGGCAACCCTAGTCTG 3’
CXCL8 - Reverse	5’ GTGAGGTAAGATGGTGGCTAAT 3’
IL-1β - Forward	5’ CTCTCACCTCTCCTACTCACTT 3’
IL-1β - Reverse	5’ TCAGAATGTGGGAGCGAATG 3’
COX-2 - Forward	5’ CCCTTGGGTGTCAAAGGTAA 3’
COX-2 - Reverse	5’ GCCCTCGCTTATGATCTGTC 3’

Supplemental Figure Legends

1275 **Figure S1: KapB expression promotes PB disassembly but does not prevent PB assembly.**
1276 HeLa cells expressing a doxycycline-inducible GFP-Dcp1a were used to determine whether
1277 KapB prevented granule assembly or promoted disassembly. A: HeLa cells were transfected with
1278 either KapB or an empty vector control prior to inducing expression of GFP-Dcp1a with
1279 doxycycline (1 µg/mL). Cells were fixed 12 h post-induction and immunostained for Hedls (PBs,
1280 red) and KapB (blue). Scale bar=20 µm. B: GFP-Dcp1a expression was induced with
1281 doxycycline (1 µg/mL) in HeLa cells prior to transfection with either KapB or an empty vector
1282 control. Cells were fixed 12 h post-transfection and immunostained for Hedls (PBs, red) and
1283 KapB (blue). Scale bar=20 µm.
1284 **Figure S2: Canonical autophagy knockdown prevents KapB-mediated PB disassembly.**
1285 A&B: HUVECs were sequentially transduced: first with recombinant lentiviruses expressing
1286 either shRNAs targeting Atg5 or Atg14 (shAtg5, shAtg14) or a non-targeting control (NS) and
1287 selected with puromycin (1 µg/mL), and second with either KapB or an empty vector control and
1288 selected with blasticidin (5 µg/mL). Samples were lysed in 2x Laemmli and resolved by SDS-
1289 PAGE. Samples were immunoblotted for Atg5 (A) or Atg14 (B). For Atg5 (A), representative
1290 blot is from the same membrane, hashed line indicates skipped lanes. For Atg5 (A) samples were
1291 quantified by normalizing Atg5 protein levels to the total protein in each lane using Image Lab
1292 (Biorad) and then to Vector NS. Results were plotted in GraphPad, a 2-way ANOVA was
1293 performed, ±SEM; n=3, ***=P<0.001. C: Atg5 +/+ (WT) and -/- (KO) MEFs were transduced as
1294 in A and harvested in 2x Laemmli buffer before being resolved by SDS-PAGE. Samples were
1295 probed for LC3, a representative blot is shown. D: Atg5 +/+ and -/- MEFs were transduced with
1296 recombinant viruses expressing KapB or an empty vector control and selected with blasticidin (5
1297 µg/mL). Samples were fixed in 4% paraformaldehyde and permeabilized in 0.1% Triton X-100.

1298 Immunofluorescence was performed for Hedls (PBs, white) and DAPI (nuclei, blue). Scale
1299 bar=20 µm. Hedls puncta were quantified using CellProfiler and presented as number of Hedls
1300 puncta per cell, all cells counted are displayed. Results were plotted in GraphPad and a 2-way
1301 ANOVA was performed on the main column effects with a Tukey's multiple comparison test,
1302 bar represents the mean; n=3, **=P<0.01.
1303
1304 **Figure S3: Canonical autophagy shRNA silencing in HeLa cells.** A&B: HeLas were
1305 transduced with recombinant lentiviruses expressing either shRNAs targeting Atg5 or Atg14
1306 (shAtg5, shAtg14) or a non-targeting control (NS) and selected with puromycin (1 µg/mL) prior
1307 to transfection with KapB or an empty vector for luciferase assays. Samples were lysed in 2x
1308 Laemmli buffer and resolved by SDS-PAGE before immunoblotting with Atg5 (A) or Atg14 (B).
1309 Representative blots are shown.
1310
1311 **Figure S4: Selective autophagy receptor knockdown in HUVECs reveals that OPTN and**
1312 **p62 are not required for KapB-mediated PB disassembly.** A&B: HUVECs were transduced
1313 with shRNAs targeting VCP, NBR1, or a non-targeting control (NS) and selected with
1314 puromycin (1 µg/mL), then transduced with an empty vector control or KapB and selected with
1315 blasticidin (5 µg/mL). Samples were lysed in 2x Laemmli buffer, resolved by SDS-PAGE, and
1316 immunoblotted for NBR1 (A) and VCP (B). Representative blots are shown, successful VCP
1317 knockdown was lethal, while NBR1 knockdown was not successful. C: HUVECs were
1318 transduced with shRNAs targeting NDP52 or a non-targeting control (NS) and selected with
1319 puromycin (1 µg/mL), then transduced with an empty vector control or KapB and selected with
1320 blasticidin (5 µg/mL). Samples were lysed in 2x Laemmli buffer, resolved by SDS-PAGE, and

1321 immunoblotted for NDP52. D&E: HUVECs were transduced with shRNAs targeting p62,
1322 OPTN, or a non-targeting control (NS) and selected with puromycin (1 µg/mL), then transduced
1323 with an empty vector control or KapB and selected with blasticidin (5 µg/mL). Samples were
1324 lysed in 2x Laemmli buffer and resolved by SDS-PAGE. Samples were immunoblotted for p62
1325 (D) and OPTN (E), representative blots are shown. F: HUVECs were transduced as in D and E.
1326 Coverslips were fixed in 4% paraformaldehyde, permeabilized in 0.1% Triton X-100 and
1327 immunostained for Hedls (PBs; white), DAPI (nuclei, blue). Scale bar=20 µm. Hedls puncta
1328 were quantified using CellProfiler and presented as number of Hedls puncta per cell, all cells
1329 counted are displayed. Results were plotted in GraphPad and a 2-way ANOVA was performed
1330 on the main column effects with a Tukey's multiple comparison test, bar represents the mean;
1331 n=3, **=P<0.01. G: HUVECs were transduced with recombinant lentiviruses targeting NDP52
1332 or a non-targeting control (NS) and selected with puromycin (1 µg/mL). Samples were lysed in
1333 2x Laemmli buffer, resolved by SDS-PAGE, and immunoblotted for NDP52 to confirm
1334 knockdown for paired Torin immunofluorescence experiments.
1335
1336 **Figure S5: shRNA silencing of selective autophagy receptors in HeLa cells.** A, B&C: HeLas
1337 were transduced with shRNAs targeting NDP52, OPTN, p62, or a non-targeting control (NS) and
1338 selected with puromycin (1 µg/mL) prior to transfection with KapB or an empty vector for
1339 luciferase assays. Samples were lysed in 2x Laemmli buffer, resolved by SDS-PAGE, and
1340 immunoblotted for NDP52 (A), p62 (B), and OPTN (C). Representative blots are shown.
1341
1342 **Figure S6: NDP52 shRNA silencing and rescue in control HUVECs.** A: Representative
1343 western blot of HUVECs transduced with an shRNA targeting the 3'UTR of NDP52 or a non-

1344 targeting control (NS) and selected with puromycin (1 µg/mL), then co-transduced with an
1345 empty vector control and mCherry (mCh) or KapB and mCh. Samples were lysed in 2x
1346 Laemmli, resolved by SDS-PAGE, and immunoblotted for NDP52. B: HUVECs were
1347 sequentially transduced first with recombinant lentivirus expressing shDNP52 targeting the 3'-
1348 UTR of NDP52 or a NS control and selected with blasticidin (5 µg/mL), and second, with vector
1349 and either an mCherry control (mCh) or RFP-NDP52. Coverslips were fixed with 4% v/v
1350 paraformaldehyde, permeabilized with 0.1% Triton X-100, and were immunostained with Hedls
1351 (PBs, green). Scale bar=20 µm. C: Hedls puncta were quantified using CellProfiler and presented
1352 as number of Hedls puncta per cell, all cells counted are displayed. Results were plotted in
1353 GraphPad and a 2-way ANOVA was performed on the main column effects with a Tukey's
1354 multiple comparison test, bar represents the mean; n=3.
1355

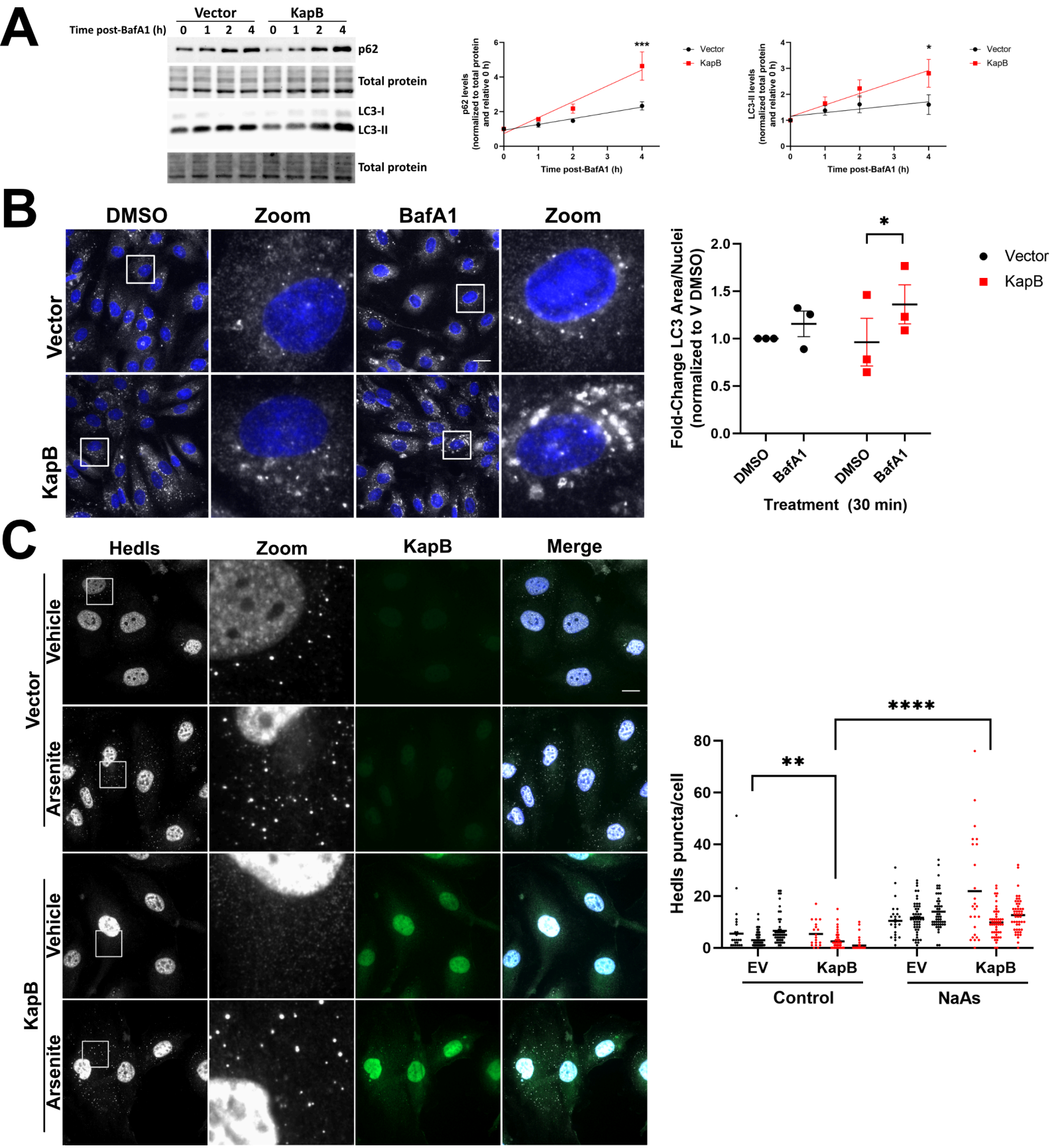
A
Vector
KapB
Time post-BafA1 (h)
0 1 2 4 0 1 2 4
p62
Total protein
LC3-I
LC3-II
Total protein
p62 levels (normalized to total protein and relative 0 h)
Time post-BafA1 (h)
***
Vector
KapB
LC3-II levels (normalized total protein and relative 0 h)
Time post-BafA1 (h)
*
Vector
KapB
B
DMSO
Zoom
BafA1
Zoom
Vector
KapB
Fold-Change LC3 Area/Nuclei (normalized to V DMSO)
*
Vector
KapB
DMSO
BafA1
DMSO
BafA1
Treatment (30 min)
C
HedIs
Zoom
KapB
Merge
Vector
Vehicle
Arsenite
KapB
Vehicle
Arsenite
HedIs puncta/cell
**
****
EV
KapB
EV
KapB
Control
NaAs

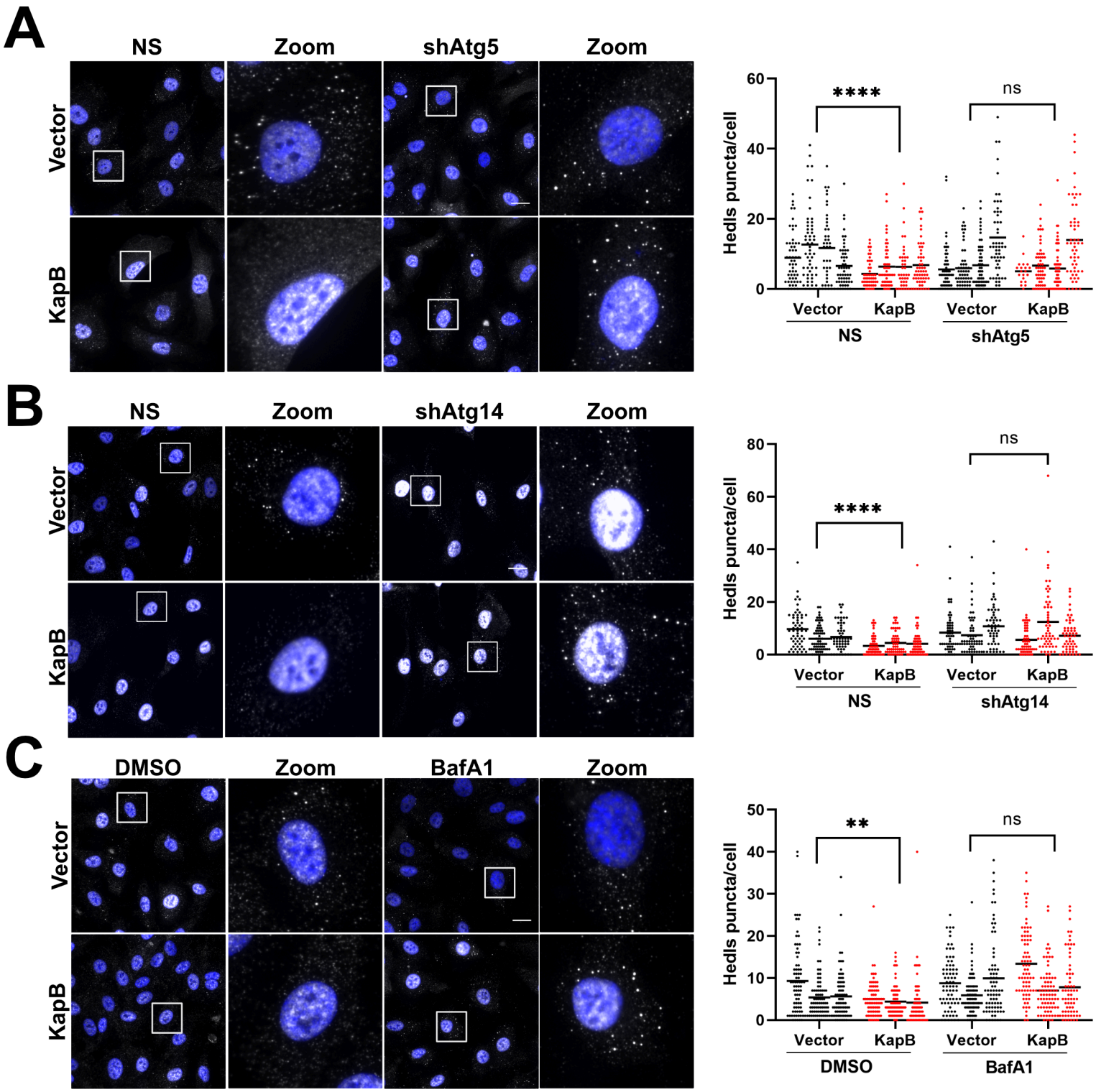
A
NS
Zoom
shAtg5
Zoom
Vector
KapB
Hedls puncta/cell
60
40
20
0
****
ns
Vector
KapB
Vector
KapB
NS
shAtg5
B
NS
Zoom
shAtg14
Zoom
Vector
KapB
Hedls puncta/cell
80
60
40
20
0
****
ns
Vector
KapB
Vector
KapB
NS
shAtg14
C
DMSO
Zoom
BafA1
Zoom
Vector
KapB
Hedls puncta/cell
50
40
30
20
10
0
**
ns
Vector
KapB
Vector
KapB
DMSO
BafA1

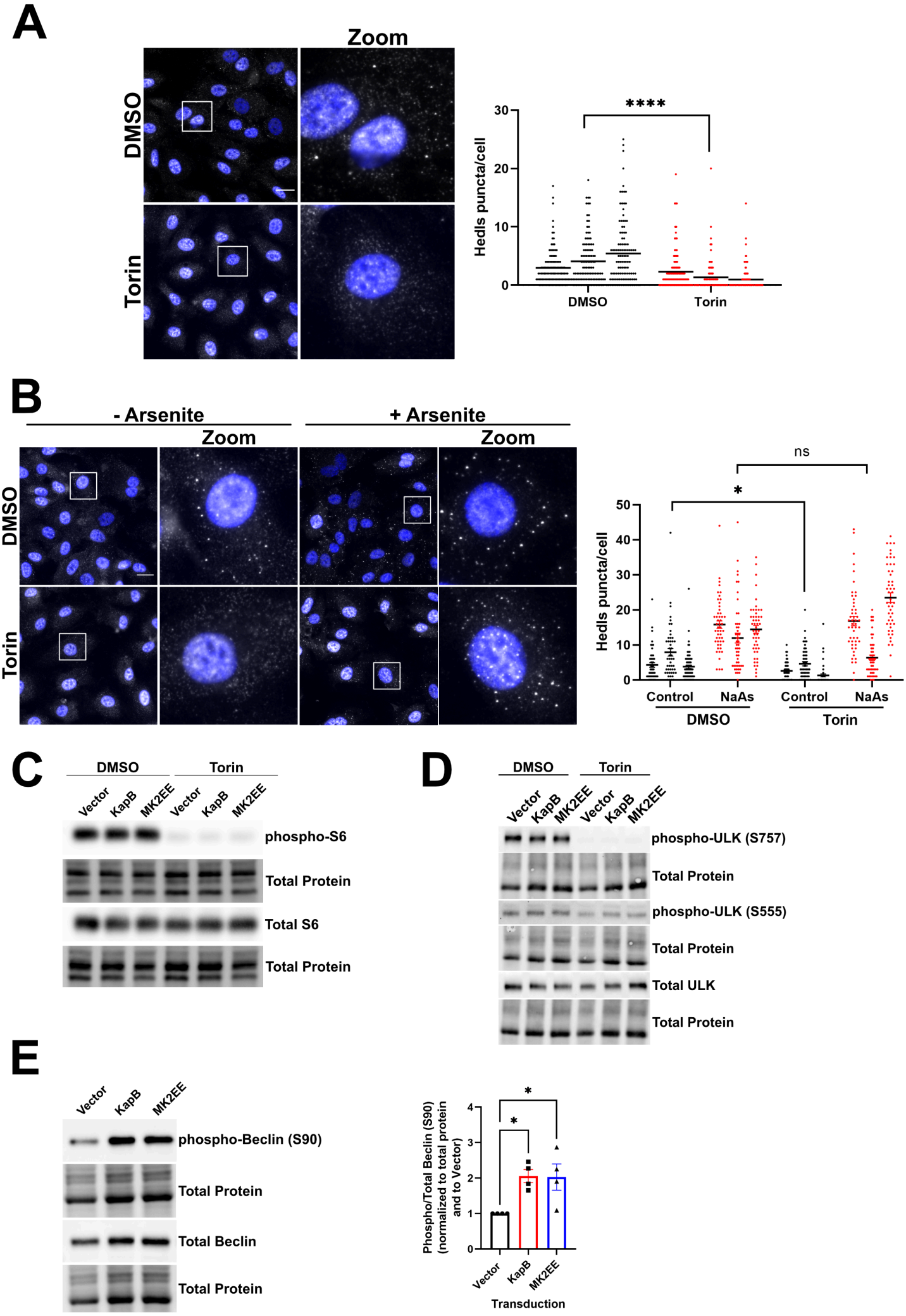
A
Zoom
DMSO
Torin
****
Hedls puncta/cell
30
20
10
0
DMSO
Torin
B
- Arsenite
+ Arsenite
Zoom
Zoom
DMSO
Torin
ns
*
Hedls puncta/cell
50
40
30
20
10
0
Control
NaAs
Control
NaAs
DMSO
Torin
C
DMSO
Torin
Vector
KapB
MK2EE
Vector
KapB
MK2EE
phospho-S6
Total Protein
Total S6
Total Protein
D
DMSO
Torin
Vector
KapB
MK2EE
Vector
KapB
MK2EE
phospho-ULK (S757)
Total Protein
phospho-ULK (S555)
Total Protein
Total ULK
Total Protein
E
Vector
KapB
MK2EE
phospho-Beclin (S90)
Total Protein
Total Beclin
Total Protein
*
*
Phospho/Total Beclin (S90)
(normalized to total protein
and to Vector)
4
3
2
1
0
Vector
KapB
MK2EE
Transduction

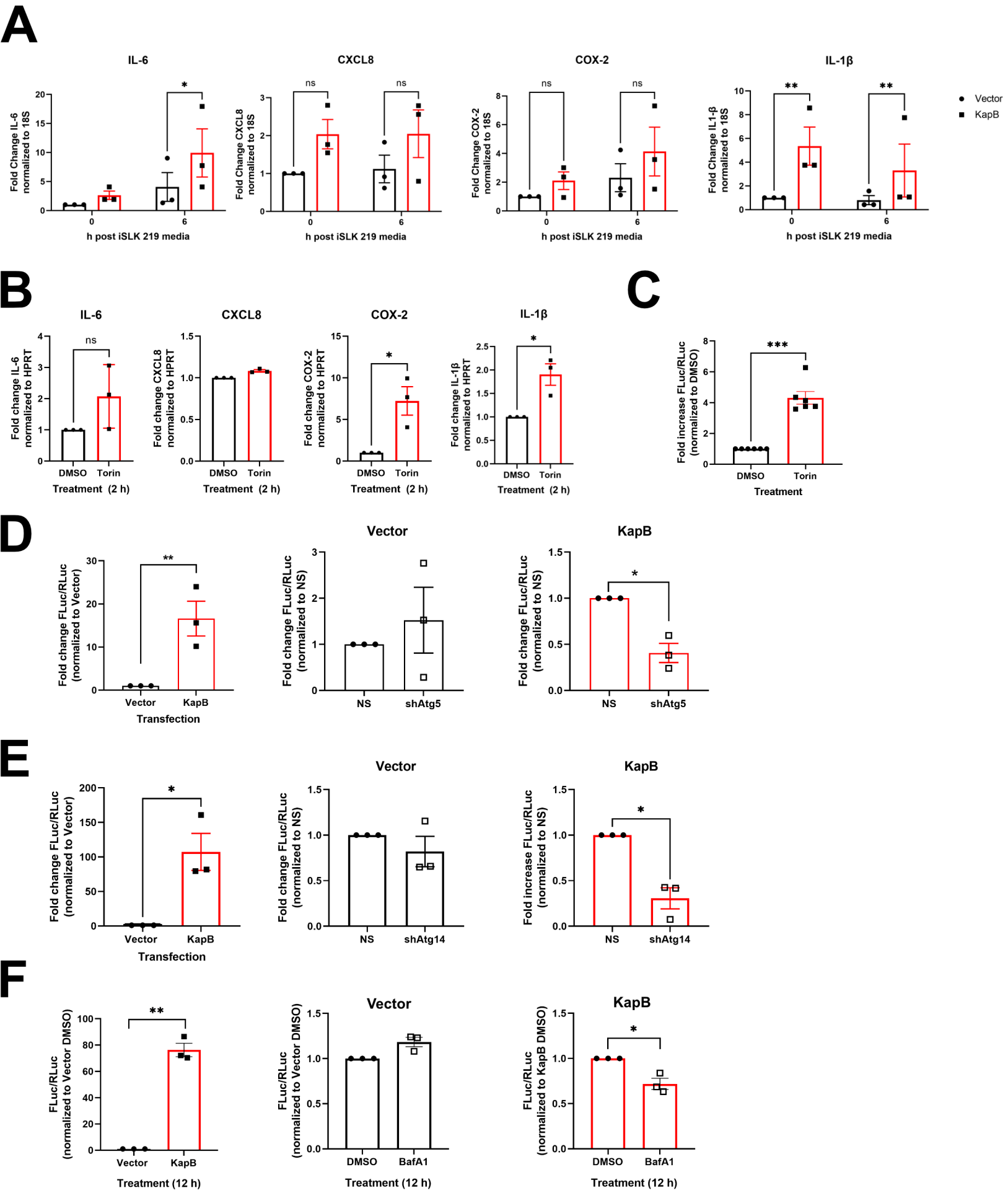
A
IL-6
CXCL8
COX-2
IL-1β
Fold Change IL-6 normalized to 18S
Fold Change CXCL8 normalized to 18S
Fold Change COX-2 normalized to 18S
Fold Change IL1-β normalized to 18S
h post iSLK 219 media
Vector
KapB
B
Fold change IL-6 normalized to HPRT
Fold change CXCL8 normalized to HPRT
Fold change COX-2 normalized to HPRT
Fold change IL-1β normalized to HPRT
DMSO
Torin
Treatment (2 h)
C
Fold increase FLuc/RLuc (normalized to DMSO)
Treatment
D
Fold change FLuc/RLuc (normalized to Vector)
Transfection
Fold change FLuc/RLuc (normalized to NS)
NS
shAtg5
E
Fold increase FLuc/RLuc (normalized to NS)
shAtg14
F
FLuc/RLuc (normalized to Vector DMSO)
FLuc/RLuc (normalized to Vector DMSO)
FLuc/RLuc (normalized to KapB DMSO)
BafA1
Treatment (12 h)

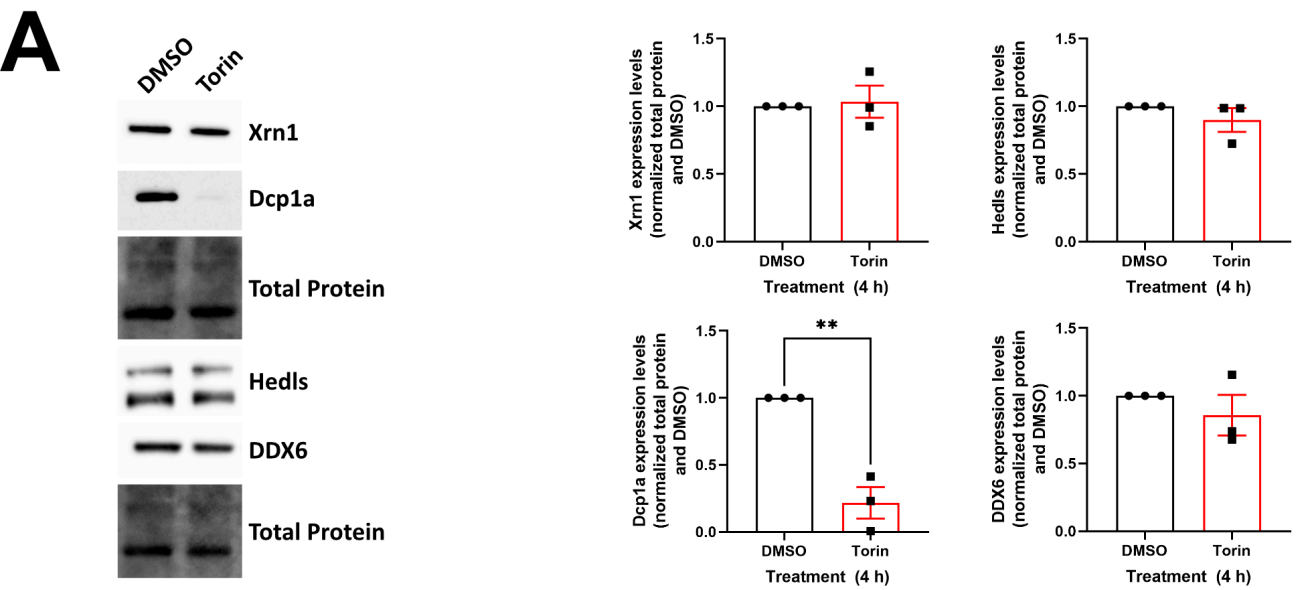
A
DMSO
Torin
Xrn1
Dcp1a
Total Protein
Hedls
DDX6
Total Protein
Xrn1 expression levels (normalized total protein and DMSO)
Hedls expression levels (normalized total protein and DMSO)
Dcp1a expression levels (normalized total protein and DMSO)
DDX6 expression levels (normalized total protein and DMSO)
1.5
1.0
0.5
0.0
**
DMSO
Torin
Treatment (4 h)

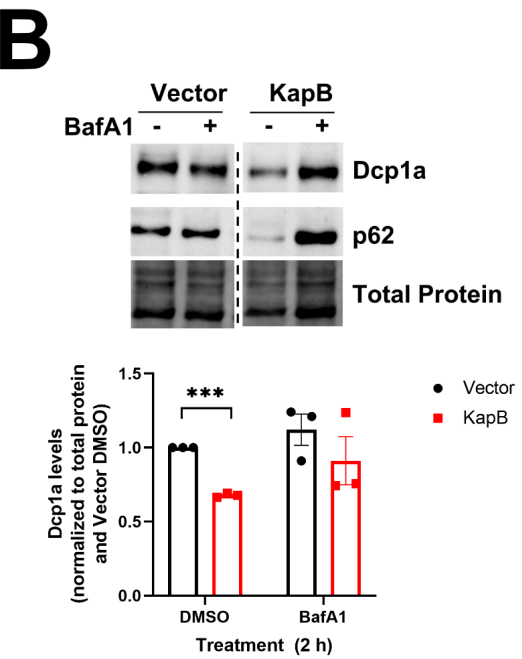
B
Vector
KapB
BafA1
-
+
-
+
Dcp1a
p62
Total Protein
Dcp1a levels (normalized to total protein and Vector DMSO)
1.5
1.0
0.5
0.0
***
Vector
KapB
DMSO
BafA1
Treatment (2 h)

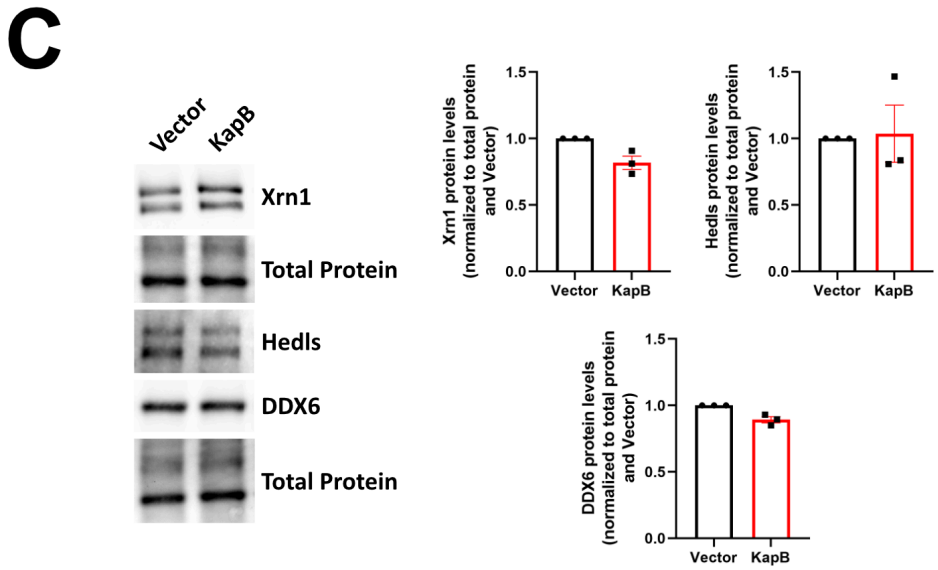
C
Vector
KapB
Xrn1
Total Protein
Hedls
DDX6
Total Protein
Xrn1 protein levels (normalized to total protein and Vector)
Hedls protein levels (normalized to total protein and Vector)
DDX6 protein levels (normalized to total protein and Vector)
1.5
1.0
0.5
0.0
Vector
KapB

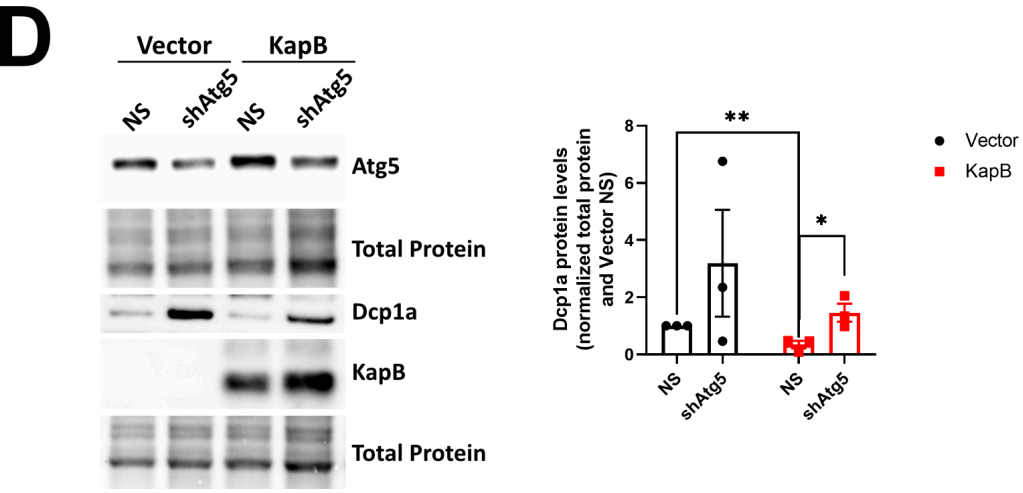
D
Vector
KapB
NS
shAtg5
NS
shAtg5
Atg5
Total Protein
Dcp1a
KapB
Total Protein
Dcp1a protein levels (normalized total protein and Vector NS)
8
6
4
2
0
**
*
Vector
KapB
NS
shAtg5
NS
shAtg5

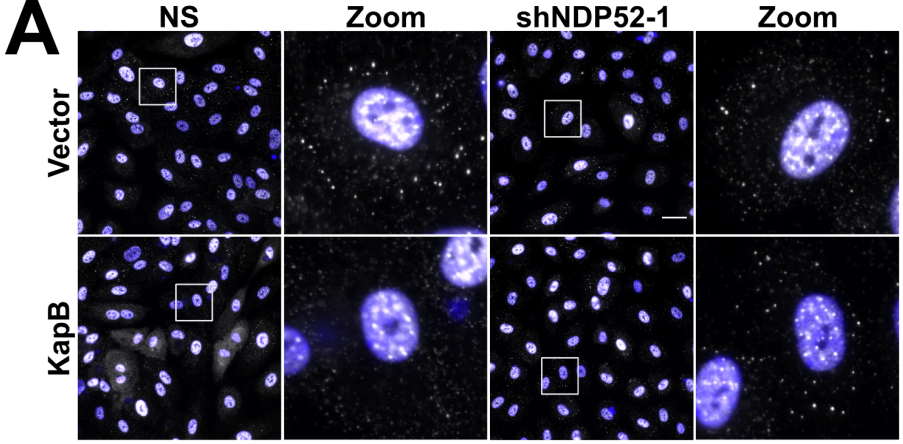
A
NS
Zoom
shNDP52-1
Zoom
Vector
KapB

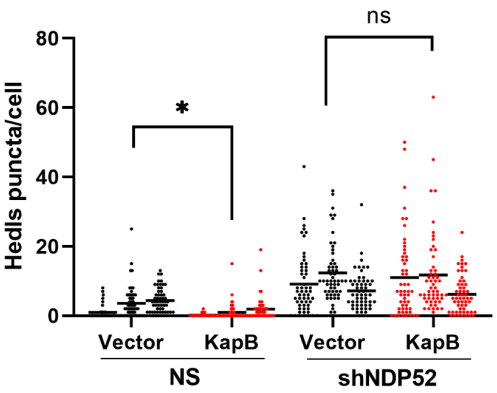
Hedls puncta/cell
80
60
40
20
0
*
ns
Vector
KapB
Vector
KapB
NS
shNDP52

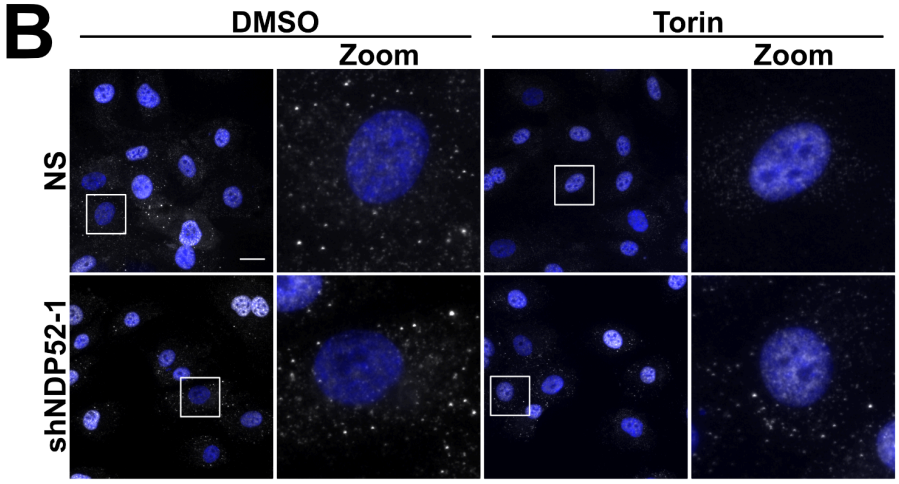
B
DMSO
Torin
Zoom
Zoom
NS
shNDP52-1

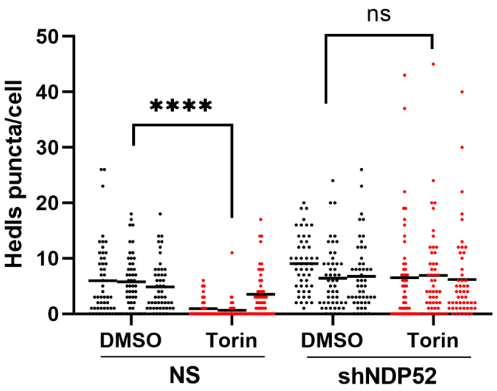
Hedls puncta/cell
50
40
30
20
10
0
****
ns
DMSO
Torin
DMSO
Torin
NS
shNDP52

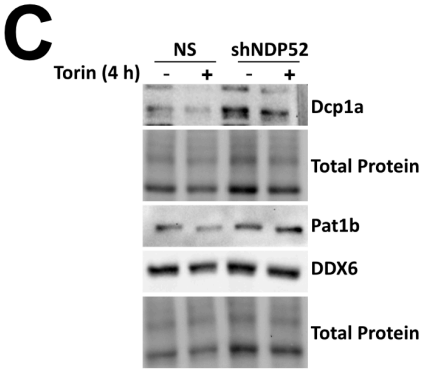
C
NS
shNDP52
Torin (4 h)
-
+
-
+
Dcp1a
Total Protein
Pat1b
DDX6
Total Protein

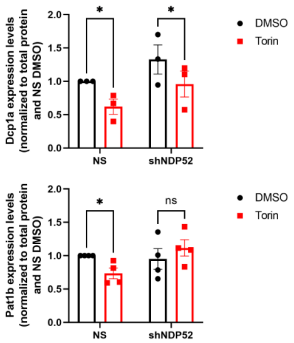
Dcp1a expression levels (normalized to total protein and NS DMSO)
2.0
1.5
1.0
0.5
0.0
*
*
NS
shNDP52
DMSO
Torin
Pat1b expression levels (normalized to total protein and NS DMSO)
*
ns
NS
shNDP52
DMSO
Torin

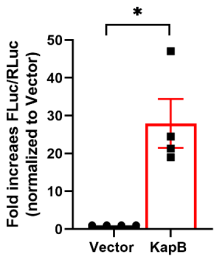
D
Fold increaes FLuc/RLuc (normalized to Vector)
50
40
30
20
10
0
*
Vector
KapB

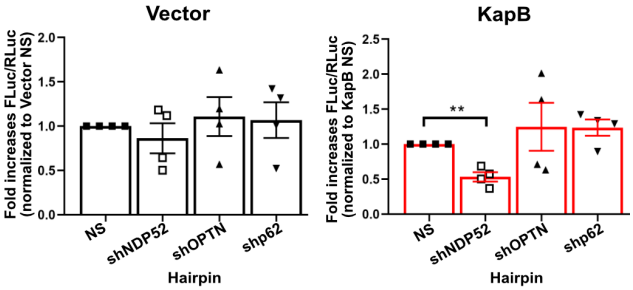
Vector
KapB
Fold increases FLuc/RLuc (normalized to Vector NS)
2.0
1.5
1.0
0.5
0.0
Fold increases FLuc/RLuc (normalized to KapB NS)
2.5
2.0
1.5
1.0
0.5
0.0
**
NS
shNDP52
shOPTN
shp62
Hairpin

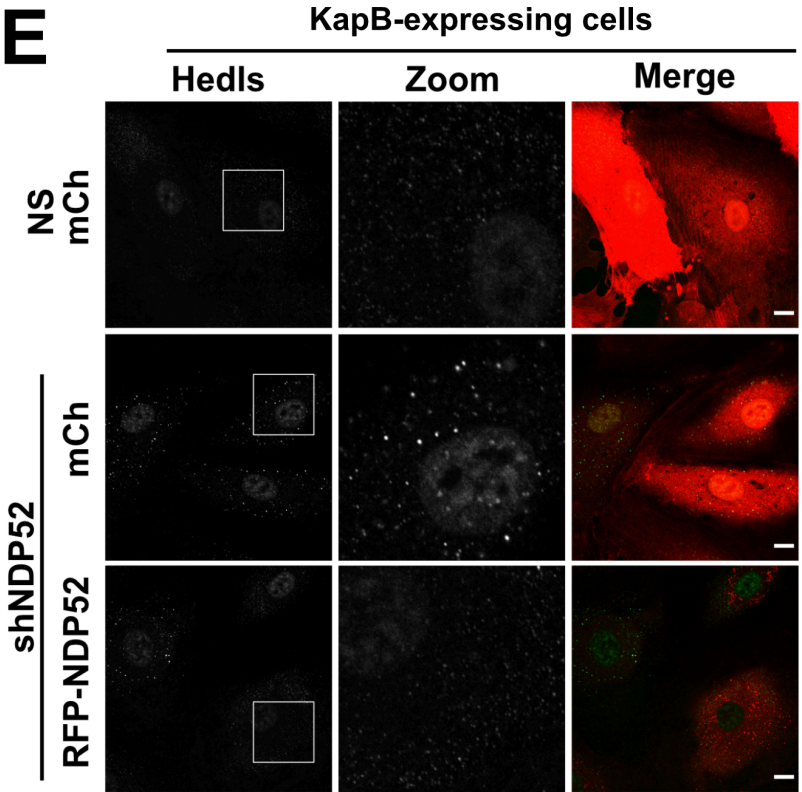
E
KapB-expressing cells
Hedls
Zoom
Merge
NS mCh
shNDP52
mCh
RFP-NDP52

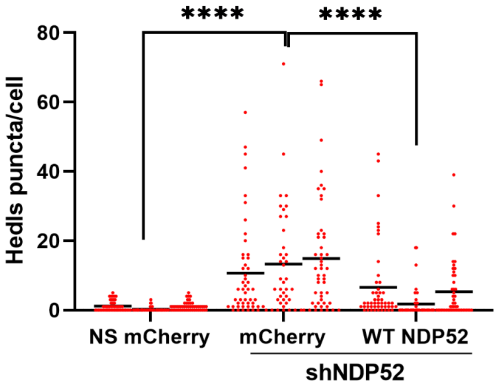
F
Hedls puncta/cell
80
60
40
20
0
****
****
NS mCherry
mCherry
WT NDP52
shNDP52

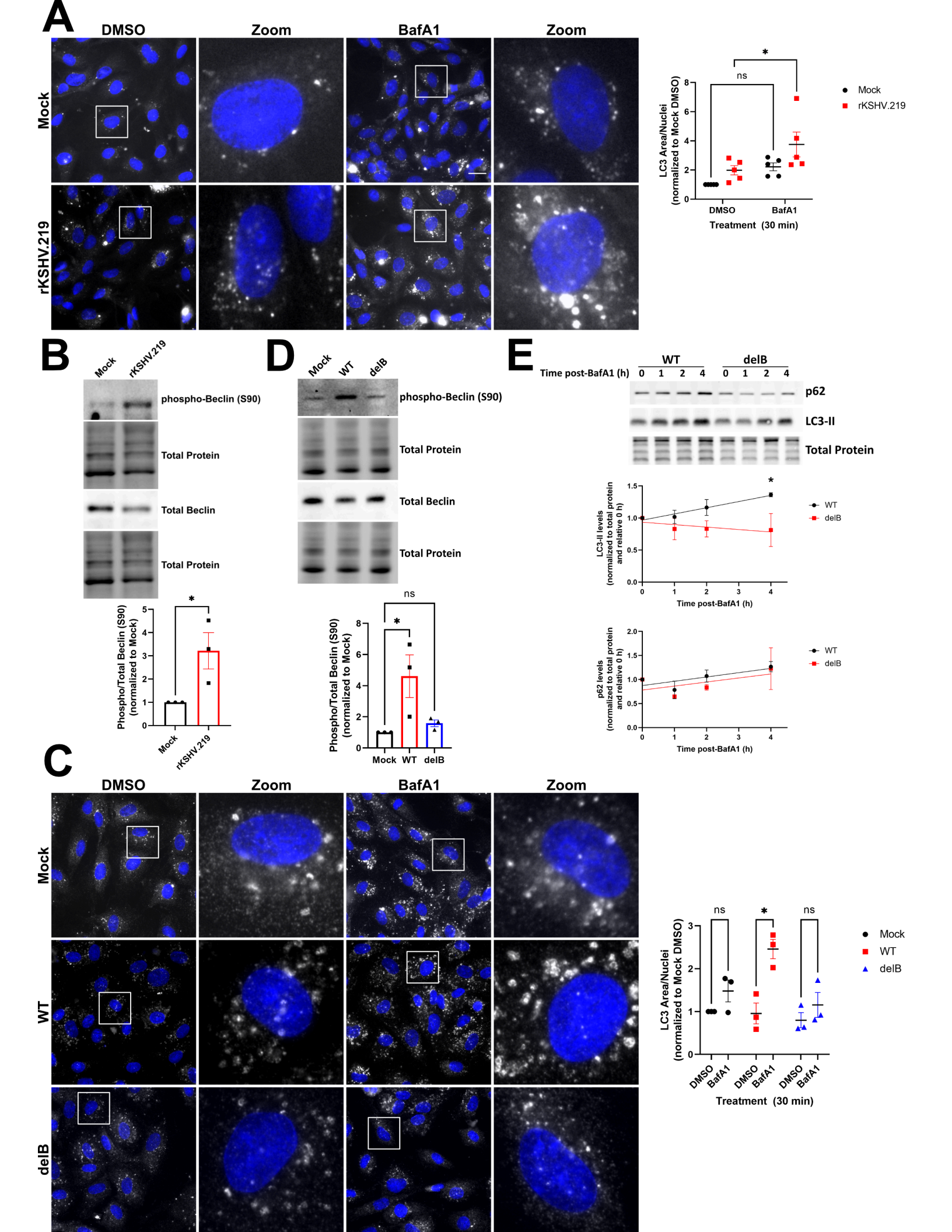
A
DMSO
Zoom
BafA1
Zoom
Mock
rKSHV.219
LC3 Area/Nuclei (normalized to Mock DMSO)
ns
*
Mock
rKSHV.219
DMSO
BafA1
Treatment (30 min)
B
Mock
rKSHV.219
phospho-Beclin (S90)
Total Protein
Total Beclin
Total Protein
Phospho/Total Beclin (S90) (normalized to Mock)
*
Mock
rKSHV.219
D
Mock
WT
delB
phospho-Beclin (S90)
Total Protein
Total Beclin
Total Protein
Phospho/Total Beclin (S90) (normalized to Mock)
ns
*
Mock
WT
delB
E
WT
delB
Time post-BafA1 (h)
0 1 2 4
0 1 2 4
p62
LC3-II
Total Protein
LC3-II levels (normalized to total protein and relative 0 h)
*
WT
delB
Time post-BafA1 (h)
p62 levels (normalized to total protein and relative 0 h)
WT
delB
Time post-BafA1 (h)
C
DMSO
Zoom
BafA1
Zoom
Mock
WT
delB
LC3 Area/Nuclei (normalized to Mock DMSO)
ns
*
ns
Mock
WT
delB
DMSO
BafA1
DMSO
BafA1
DMSO
BafA1
Treatment (30 min)

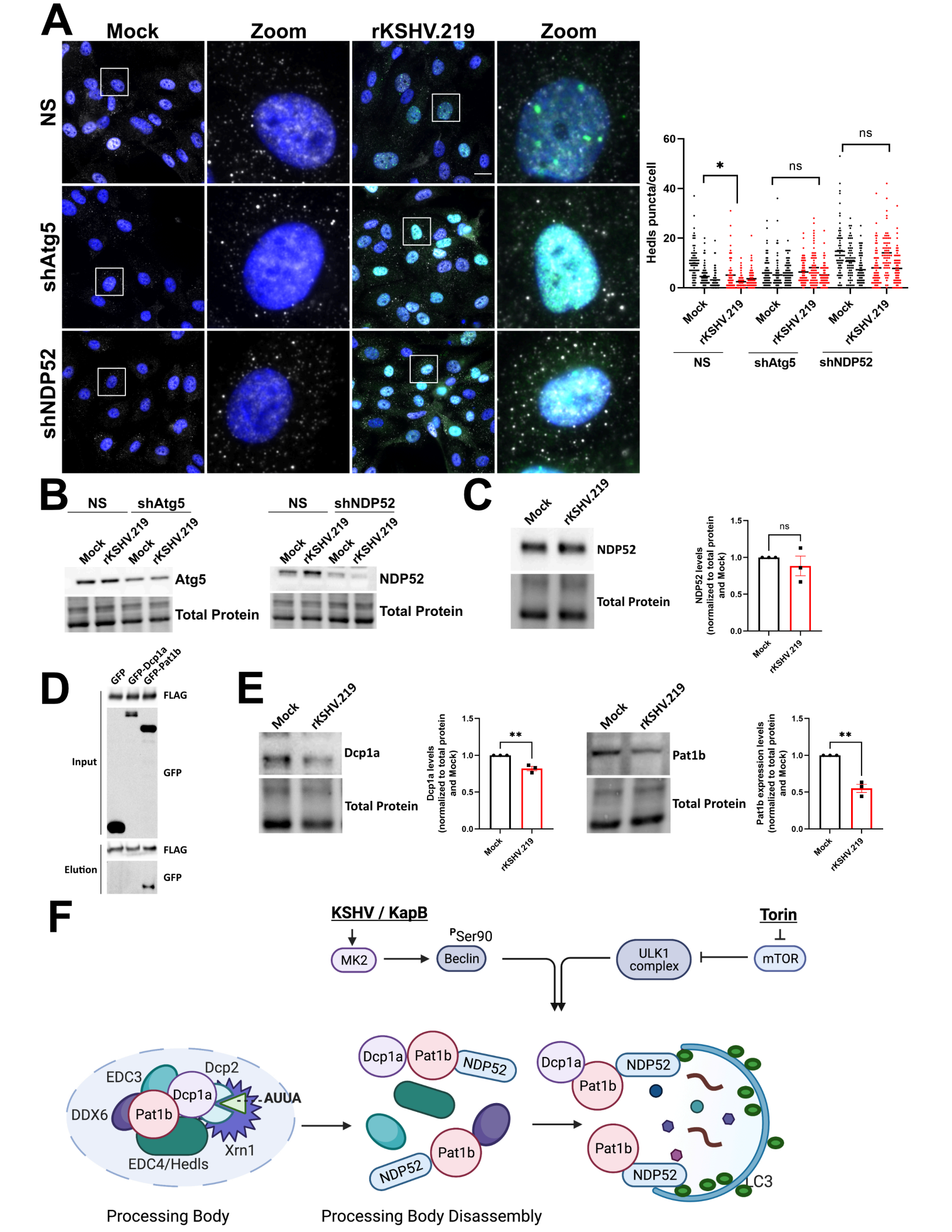
A
Mock
Zoom
rKSHV.219
Zoom
NS
shAtg5
shNDP52
Hedls puncta/cell
60
40
20
0
*
ns
ns
Mock
rKSHV.219
Mock
rKSHV.219
Mock
rKSHV.219
NS
shAtg5
shNDP52
B
NS
shAtg5
Mock
rKSHV.219
Mock
rKSHV.219
Atg5
Total Protein
NS
shNDP52
Mock
rKSHV.219
Mock
rKSHV.219
NDP52
Total Protein
C
Mock
rKSHV.219
NDP52
Total Protein
NDP52 levels (normalized to total protein and Mock)
1.5
1.0
0.5
0.0
ns
Mock
rKSHV.219
D
GFP
GFP-Dcp1a
GFP-Pat1b
FLAG
Input
GFP
FLAG
Elution
GFP
E
Mock
rKSHV.219
Dcp1a
Total Protein
Dcp1a levels (normalized to total protein and Mock)
1.5
1.0
0.5
0.0
**
Mock
rKSHV.219
Mock
rKSHV.219
Pat1b
Total Protein
Pat1b expression levels (normalized to total protein and Mock)
1.5
1.0
0.5
0.0
**
Mock
rKSHV.219
F
KSHV / KapB
MK2
PSer90
Beclin
ULK1 complex
Torin
mTOR
EDC3
Dcp2
Dcp1a
DDX6
Pat1b
AUUA
Xrn1
EDC4/Hedls
Processing Body
Dcp1a
Pat1b
NDP52
Pat1b
NDP52
Processing Body Disassembly
Dcp1a
NDP52
Pat1b
Pat1b
NDP52
LC3

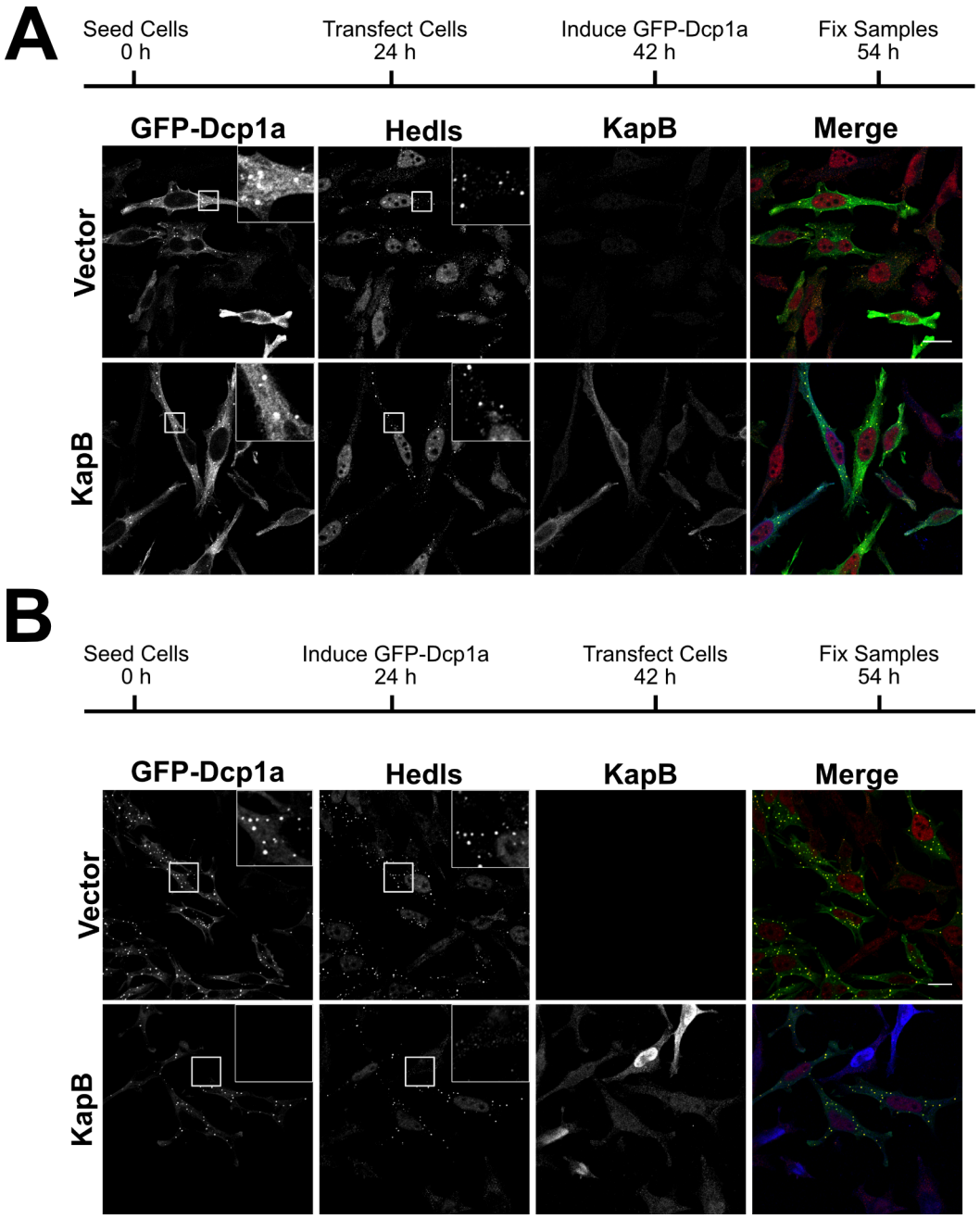
A
Seed Cells
0 h
Transfect Cells
24 h
Induce GFP-Dcp1a
42 h
Fix Samples
54 h
GFP-Dcp1a
Hedls
KapB
Merge
Vector
KapB
B
Seed Cells
0 h
Induce GFP-Dcp1a
24 h
Transfect Cells
42 h
Fix Samples
54 h
GFP-Dcp1a
Hedls
KapB
Merge
Vector
KapB

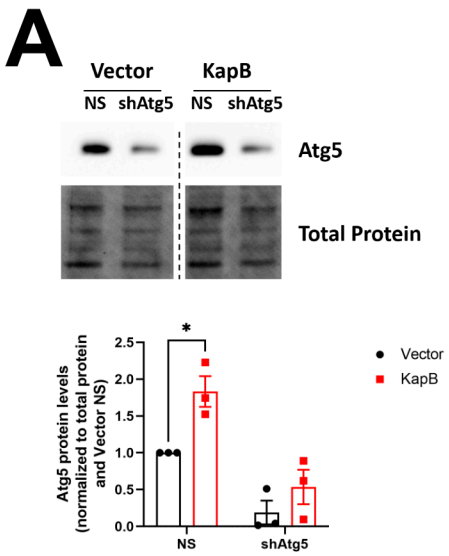
A
Vector
KapB
NS
shAtg5
NS
shAtg5
Atg5
Total Protein
Atg5 protein levels (normalized to total protein and Vector NS)
2.5
2.0
1.5
1.0
0.5
0.0
*
NS
shAtg5
Vector
KapB

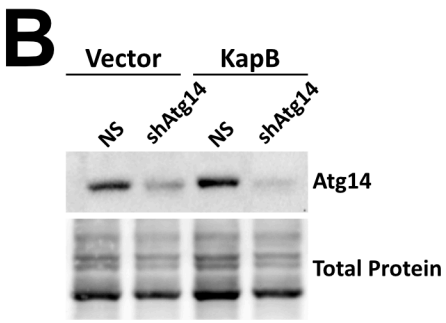
B
Vector
KapB
NS
shAtg14
NS
shAtg14
Atg14
Total Protein

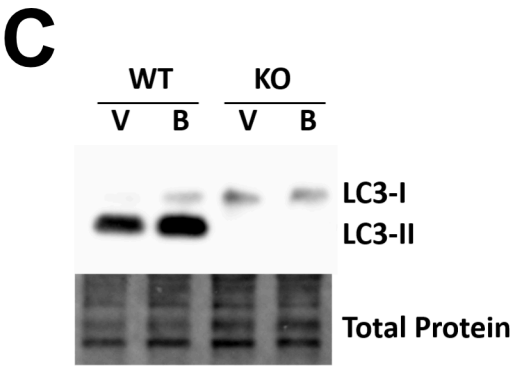
C
WT
KO
V
B
V
B
LC3-I
LC3-II
Total Protein

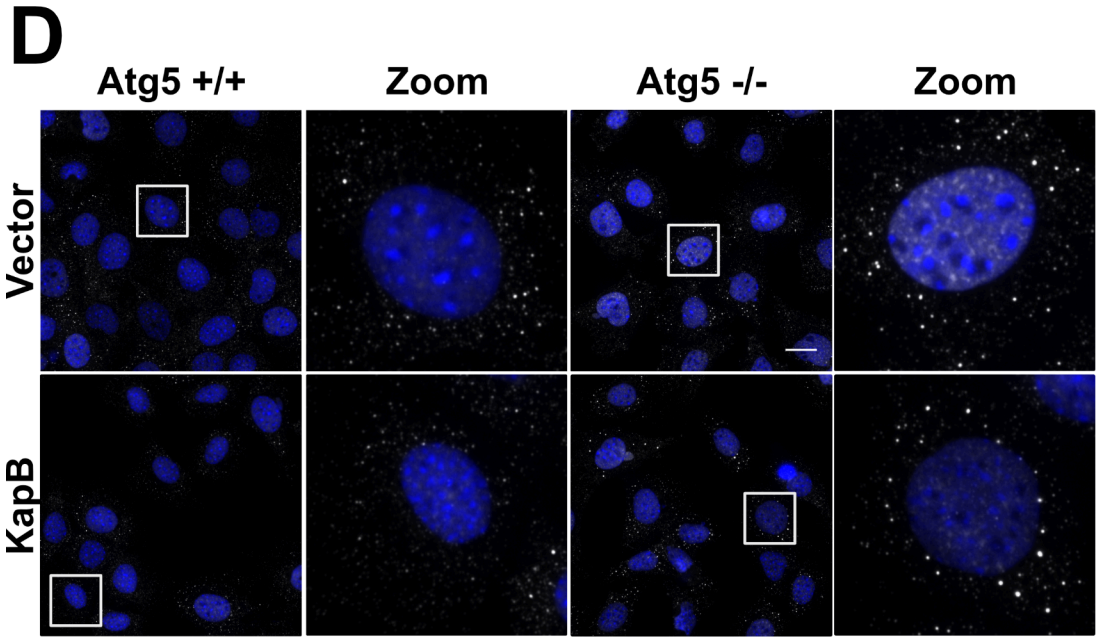
D
Atg5 +/+
Zoom
Atg5 -/-
Zoom
Vector
KapB

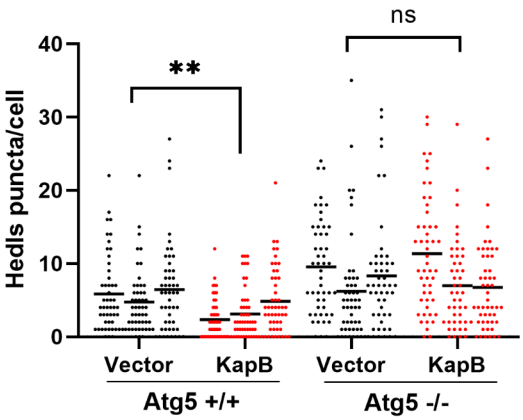
Hedls puncta/cell
40
30
20
10
0
**
ns
Vector
KapB
Vector
KapB
Atg5 +/+
Atg5 -/-

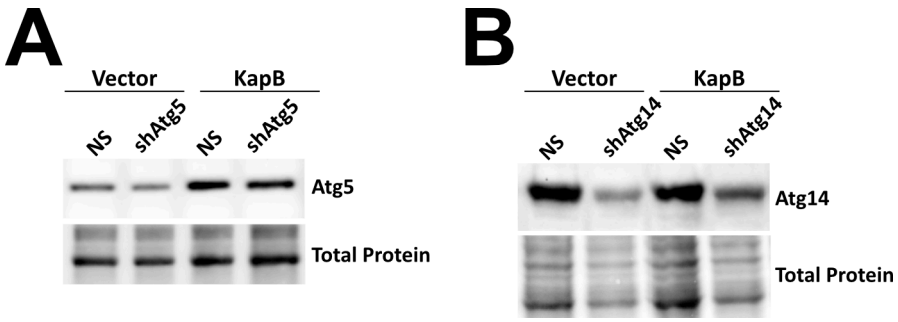
A
Vector
KapB
NS
shAtg5
NS
shAtg5
Atg5
Total Protein
B
Vector
KapB
NS
shAtg14
NS
shAtg14
Atg14
Total Protein

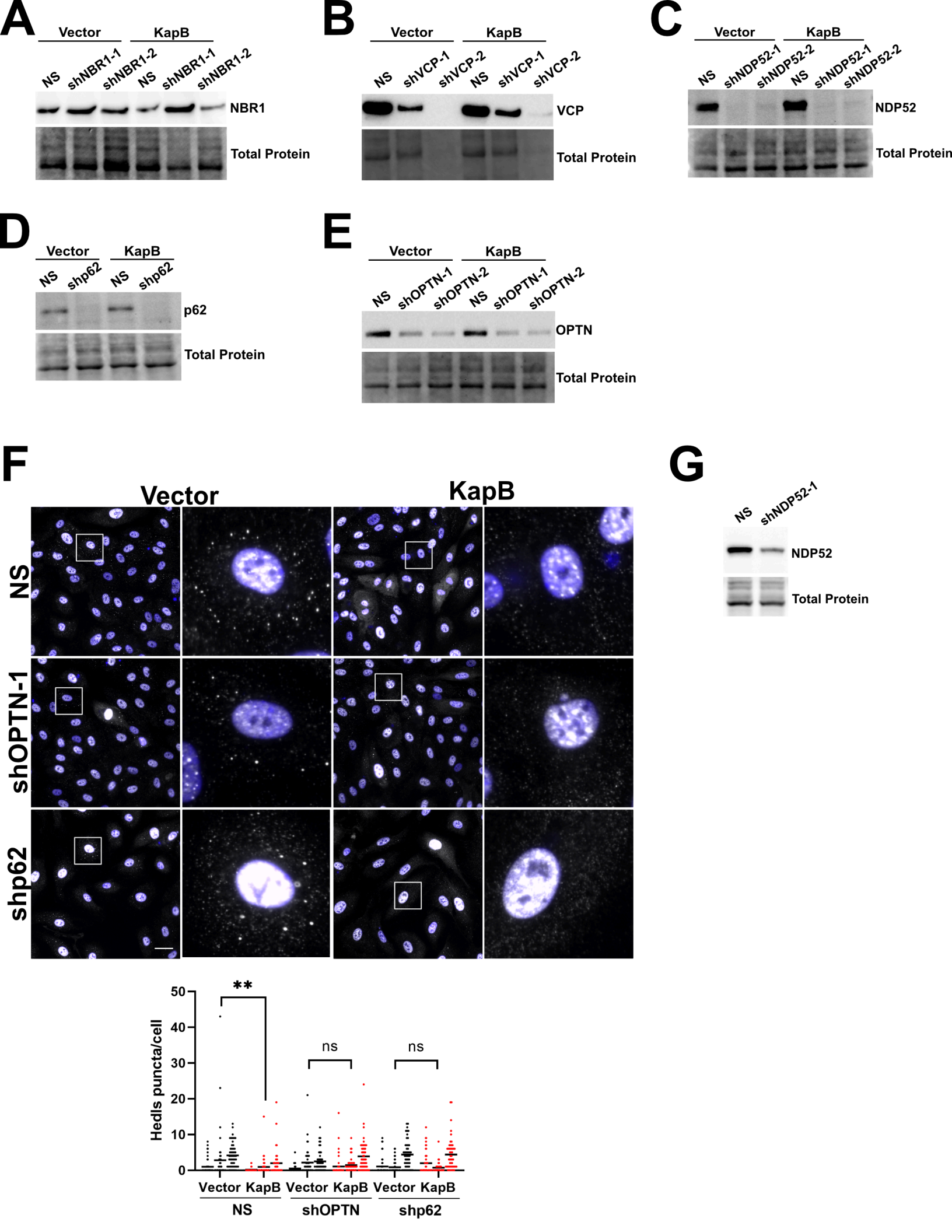
A
Vector
KapB
NS
shNBR1-1
shNBR1-2
NS
shNBR1-1
shNBR1-2
NBR1
Total Protein
B
Vector
KapB
NS
shVCP-1
shVCP-2
NS
shVCP-1
shVCP-2
VCP
Total Protein
C
Vector
KapB
NS
shNDP52-1
shNDP52-2
NS
shNDP52-1
shNDP52-2
NDP52
Total Protein
D
Vector
KapB
NS
shp62
NS
shp62
p62
Total Protein
E
Vector
KapB
NS
shOPTN-1
shOPTN-2
NS
shOPTN-1
shOPTN-2
OPTN
Total Protein
F
Vector
KapB
NS
shOPTN-1
shp62
G
NS
shNDP52-1
NDP52
Total Protein
Hedls puncta/cell
50
40
30
20
10
0
**
ns
ns
Vector KapB Vector KapB Vector KapB
NS
shOPTN
shp62

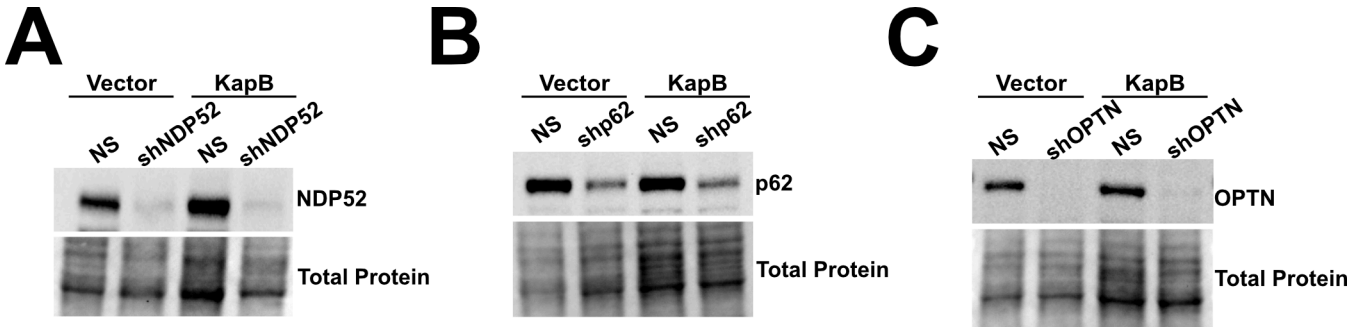
A
Vector
KapB
NS
shNDP52
NS
shNDP52
NDP52
Total Protein
B
Vector
KapB
NS
shp62
NS
shp62
p62
Total Protein
C
Vector
KapB
NS
shOPTN
NS
shOPTN
OPTN
Total Protein

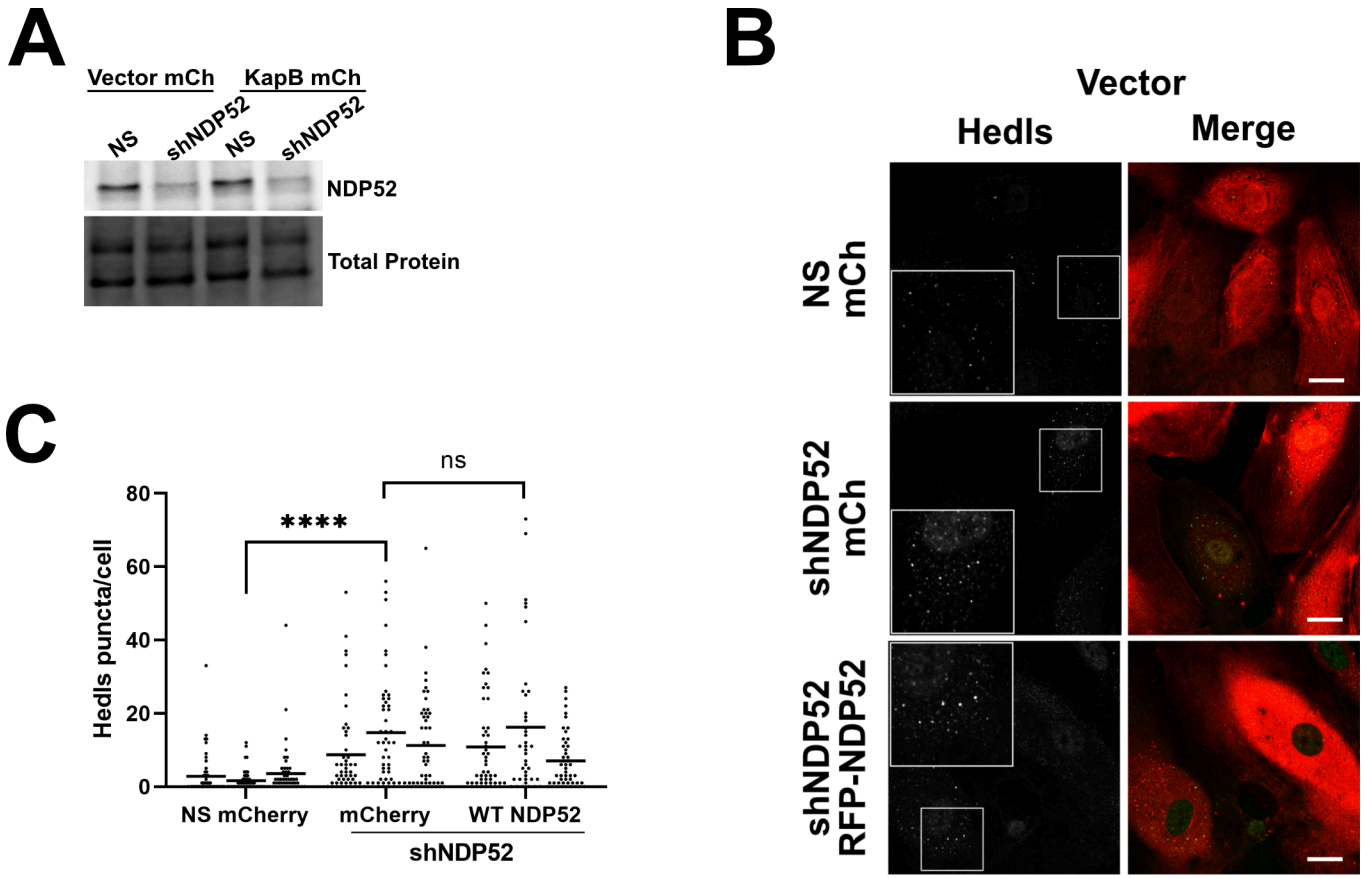
A
Vector mCh
KapB mCh
NS
shNDP52
NS
shNDP52
NDP52
Total Protein
B
Vector
HeDls
Merge
NS mCh
shNDP52 mCh
shNDP52 RFP-NDP52
C
HeDls puncta/cell
80
60
40
20
0
****
ns
NS mCherry
mCherry
WT NDP52
shNDP52